

5★ Knowledge Graph Embeddings with Projective Transformations

Mojtaba Nayyeri^{1,2}, Sahar Vahdati², Can Aykul¹, Jens Lehmann^{1,3}

¹Smart Data Analytics Group, University of Bonn, Germany

²Nature-Inspired Machine Intelligence-InfAI, Dresden, Germany

³Fraunhofer IAIS, Dresden, Germany

{nayyeri,aykul,jens.lehmann}@cs.uni-bonn.de, vahdati@infai.org, jens.lehmann@iais.fraunhofer.de

Abstract

Performing link prediction using knowledge graph embedding models has become a popular approach for knowledge graph completion. Such models employ a transformation function that maps nodes via edges into a vector space in order to measure the likelihood of the links. While mapping the individual nodes, the structure of subgraphs is also transformed. Most of the embedding models designed in Euclidean geometry usually support a *single* transformation type – often translation or rotation, which is suitable for learning on graphs with small differences in neighboring subgraphs. However, multi-relational knowledge graphs often include multiple subgraph structures in a neighborhood (e.g. combinations of path and loop structures), which current embedding models do not capture well. To tackle this problem, we propose a novel KGE model (5★E) in projective geometry, which supports *multiple* simultaneous transformations – specifically inversion, reflection, translation, rotation, and homothety. The model has several favorable theoretical properties and subsumes the existing approaches. It outperforms them on most widely used link prediction benchmarks.

Introduction

Knowledge graphs (KGs) with their graph-based knowledge representation in the form of (head,relation,tail) triples, have become a leading technology of recent years in AI-based tasks including question answering, data integration, and recommender systems (Ji et al. 2020). However, KGs are incomplete and the performance of any algorithm consuming them is affected by this problem. Knowledge graph embeddings (KGEs) are a prominent approach used for KG completion by predicting missing links. Every KGE model uses a transformation function to map entities (nodes) of the graph through relations in a vector space to score the plausibility of triples via a score function. The performance of KGE models heavily relies on the design of their score function that in turn defines the type of transformation they support. Such transformations distinguish the extent to which a model is able to learn complex motifs and patterns formed by combinations of the nodes and edges.

Most of the existing KGEs have been designed in Euclidean geometry and usually support a single transformation

type – often translation or rotation. This limits their ability in embedding KGs with complexities in subgraphs, especially when multiple structures exist in a neighborhood. An example of this situation is the presence of a path structure for a group of nodes close to a loop structure of another group in a KG (illustrated in Figure 1). The upper part of the figure shows examples of four different subgraphs containing combinations of path structures (a group of nodes connected via a relation) and loop structures (a group of nodes forming a loop via a relation). The lower part of the figure shows an exemplary visualisation of the embeddings of the entities depicted in the upper part of the figure. Let us focus on the left most example in the figure, i.e. the path to loop subgraph. In this example subgraph, a relation r_1 (e.g. *hypernym*) forms a path structure, a relation r_3 (e.g. *similar_to*) forms a loop structure and nodes in both structures are connected via a relation r_2 . A loop in the graph presentation can be preserved as a circle in a vector space, and a path as a line. Existing KGE models, such as TransE, RotatE, ComplEx and QuatE partially capture those structures in the embedding space. The lower part of the figure shows the possible embeddings of the given subgraphs preserved by the existing models. Let the nodes in the path be h_1, \dots, h_6 , the nodes in the loop be t_1, \dots, t_6 and $(h_i, r_2, t_i), i = 1, \dots, 6$, be the triples connecting those structures. When we consider the TransE model specifically, the embeddings of the tails t_1, \dots, t_6 cannot be transferred to the shape of a circle in the embedding space. This is because the following equations need to (approximately) hold according to the TransE score functions: $\mathbf{t}_1 + \mathbf{r}_3 \approx \mathbf{t}_2, \mathbf{t}_2 + \mathbf{r}_3 \approx \mathbf{t}_3, \dots, \mathbf{t}_6 + \mathbf{r}_3 \approx \mathbf{t}_1$. However, this results in $\mathbf{r}_3 = 0$. Therefore, $\mathbf{t}_1 = \mathbf{t}_2 = \dots = \mathbf{t}_6$ i.e. all entities are embedded into the same point in the embedding space rather than a circle (with positive radius). Similar derivations apply to more recent and complex models. Those limitations are due to the limited set of transformations supported by those models, which do not go beyond translation, rotation and homothety operations. Therefore, they cannot map line structures to circle structures and vice versa.

This type of limitation stems from the underlying geometry. While major existing models cover at most two transformation types, we propose a model based on projective geometry that provides a uniform way for *simultaneously* representing five *transformation types* namely translation, rotation, homothety, inversion, and reflection. The combination

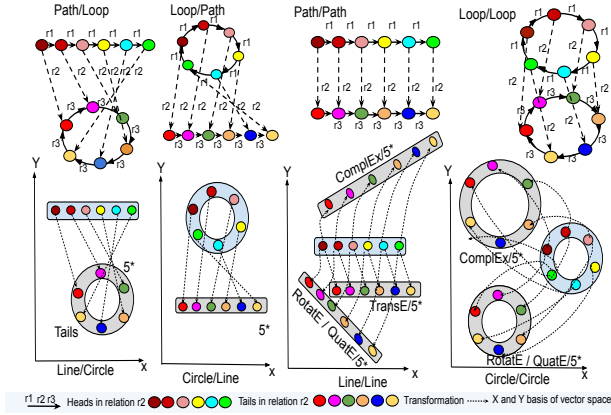


Figure 1: Graph and vector representation of path/loop.

of such transformation types results in various *transformation functions* (parabolic, circular, elliptic, hyperbolic, and loxodromic) subsumed by projective transformations. As a consequence, the embeddings can preserve the structure in the previous example and many other scenarios in which different structures exist in a neighbourhood of the KG.

Our core contribution is a new five-star embedding model, i.e. a model that simultaneously employs five transformation types and consequently can preserve various-shaped structures in the embedding space. The model subsumes several existing state-of-the-art KGE models, i.e. their score functions can be expressed as special cases of 5^*E . Overall, our model, dubbed 5^*E , is (a) capable of preserving a wider range of structures than existing models (including the path and loop combinations in Figure 1), (b) fully expressive (as defined in (Wang, Gemulla, and Li 2018)), (c) subsumes the KGE models DistMult, RotatE, pRotatE, TransE, and ComplEx (d) allows to learn composition, inverse, reflexive and symmetric relation patterns. Our evaluation shows that 5^*E outperforms existing models on standard benchmarks.

Preliminaries and Background

Knowledge Graph Embeddings

A KG is a multi-relational directed graph $\mathcal{KG} = (\mathcal{E}, \mathcal{R}, \mathcal{T})$ where \mathcal{E}, \mathcal{R} are the set of nodes (entities) and edges (relations between entities) respectively. The set $\mathcal{T} = \{(h, r, t)\} \subseteq \mathcal{E} \times \mathcal{R} \times \mathcal{E}$ contains all triples as (*head, relation, tail*), e.g. (*smartPhone, hypernym, iPhone*). In order to apply learning methods on KGs, a KGE learns vector representations of entities (\mathcal{E}) and relations (\mathcal{R}). A vector representation denoted by $(\mathbf{h}, \mathbf{r}, \mathbf{t})$ is learned by the model per triple (h, r, t) , where $\mathbf{h}, \mathbf{t} \in \mathbb{V}^{d_e}$, $\mathbf{r} \in \mathbb{V}^{d_r}$ (\mathbb{V}^d is a d -dimensional vector space). TransE (Bordes et al. 2013) considers $\mathbb{V} = \mathbb{R}$ while ComplEx (Trouillon et al. 2016) and RotatE use $\mathbb{V} = \mathbb{C}$ (complex space) and QuatE (Zhang et al. 2019) considers $\mathbb{V} = \mathbb{H}$ (quaternion space). In this paper, we choose a projective space to embed the graph i.e. $\mathbb{V} = \mathbb{CP}^1$ (a complex projective line which is introduced later). Most KGE models are defined via a relation-specific transformation function $g_r : \mathbb{V}^{d_e} \rightarrow \mathbb{V}^{d_e}$ which maps head entities to tail entities,

i.e. $g_r(\mathbf{h}) = \mathbf{t}$. On top of such a transformation function, the score function $f : \mathbb{V}^{d_e} \times \mathbb{V}^{d_r} \times \mathbb{V}^{d_e} \rightarrow \mathbb{R}$ is defined to measure the plausibility for triples: $f(\mathbf{h}, \mathbf{r}, \mathbf{t}) = p(g_r(\mathbf{h}), \mathbf{t})$. Generally, the formulation of any score function can be either $p(g_r(\mathbf{h}), \mathbf{t}) = -\|g_r(\mathbf{h}) - \mathbf{t}\|$ or $p(g_r(\mathbf{h}), \mathbf{t}) = \langle g_r(\mathbf{h}), \mathbf{t} \rangle$.

Projective Geometry

Projective geometry uses *homogeneous coordinates* which represent N -dimensional coordinates with $N + 1$ numbers (i.e. use one additional parameter). For example, a point in 2D Cartesian coordinates, $[X, Y]$ becomes $[x, y, k]$ in homogeneous coordinates where $X = x/k, Y = y/k$ (in 1-dimensional real numbers, $[X]$ becomes $[x, y]$ where $X = x/y$). The key elements of projective geometry are as follows:

A **Projective Line** is a space in which a projective geometry is defined. A projective geometry requires a point at infinity to satisfy the axiom of “two parallel lines intersect in infinity”. Therefore, an extended line $\mathbb{P}^1(\mathbb{K})$ (\mathbb{K} is a real line) is realized with \mathbb{K} and a point at infinity (which topologically is a circle). More concretely, the projective line is a set $\{[x, 1] \in \mathbb{P}^1(\mathbb{K}) | x \in \mathbb{K}\}$ with an additional member $[1 : 0]$ denoting the point at infinity. When $\mathbb{K} = \mathbb{C}$, the projective line is complex (complex projective line denoted by \mathbb{CP}^1).

The **Riemann Sphere** (illustrated in Figure 9) is an extended complex plane with a point at infinity. Precisely, it is built on a plane of complex numbers wrapped around a Sphere where poles denote 0 and ∞ . In projective geometry, a complex projective line is a Riemann Sphere which used as a tool for projective transformations.

A **Projective Transformation** is the mapping of the Riemann Sphere to itself. Let $[x : y]$ be the homogeneous coordinates of a point in \mathbb{CP}^1 . A projective transformation in \mathbb{CP}^1 is expressed by a matrix multiplication (Richter-Gebert 2011; Salomon 2007) as $\tau : \mathbb{CP}^1 \rightarrow \mathbb{CP}^1$:

$$\tau([x, y]) = \mathfrak{S} \begin{bmatrix} x \\ y \end{bmatrix}, \quad \mathfrak{S} = \begin{bmatrix} a & b \\ c & d \end{bmatrix}, \quad (1)$$

where the matrix \mathfrak{S} must be invertible ($\det(\mathfrak{S}) \neq 0$). By identifying \mathbb{CP}^1 with $\hat{\mathbb{C}} = \mathbb{C} \cup \{\infty\}$, a projective transformation is represented by a fractional expression through a sequence of homogenization, transformation, and dehomogenization as

$$x \rightarrow \begin{bmatrix} x \\ 1 \end{bmatrix} \rightarrow \begin{bmatrix} a & b \\ c & d \end{bmatrix} \begin{bmatrix} x \\ 1 \end{bmatrix} \rightarrow \begin{bmatrix} ax + b \\ cx + d \end{bmatrix} \rightarrow \frac{ax + b}{cx + d}, \quad (2)$$

where the mapping $\vartheta : \hat{\mathbb{C}} \rightarrow \hat{\mathbb{C}}$ is defined as

$$\vartheta(x) = \frac{ax + b}{cx + d}, \quad ad - bc \neq 0. \quad (3)$$

The resulted mapping in Equation 3 describes all *Möbius transformations*.

The **Möbius Group** is the set of all Möbius transformations which is a projective linear group $PGL(2, \mathbb{C})$, i.e. the group of all 2×2 invertible matrices with the operation of matrix multiplication on a projective space. This group is the automorphism group $Aut(\hat{\mathbb{C}})$ of the Riemann Sphere $\hat{\mathbb{C}}$ or equivalently \mathbb{CP}^1 .

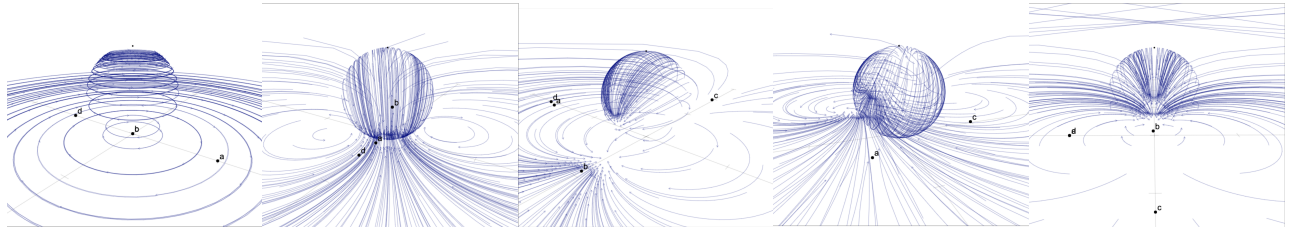


Figure 2: Transformation functions illustrated (Tim Hutton 2020) from left to right as circular, elliptic, hyperbolic, loxodromic, and parabolic. It shows a Riemann Sphere on a complex plane with one or two fix points for each function.

Variants of Möbius Transformations

Every Möbius transformation has at most two fixed points γ_1, γ_2 on the Riemann Sphere obtained by solving $\vartheta(\gamma) = \gamma$, (Richter-Gebert 2011) which gives $\gamma_{1,2} = \frac{(a-d) \pm \sqrt{\Delta}}{2c}$. Depending on the number of fixed points, Möbius transformations form parabolic or circular (one fixed point), elliptic as well as hyperbolic, and loxodromic (two fixed points) transformation functions illustrated in Figure 9. A Möbius transformation is performed on a grid by (a) a stereographic projection from complex plane to Riemann Sphere, (b) moving the Sphere, (c) stereographic projection from Sphere to plane. Each transformation has a constant $k = e^{\alpha+i\beta}$ which determines *sparsity/density* of the transformation. β is an expansion factor indicating the extent to which the fixed point γ_1 is repulsive (γ_2 is attractive). α is a rotation factor, determining the degree to which a transformation rotates the plane counter-clockwise around γ_1 (clockwise around γ_2).

Related Work

KGE models can be classified according to their embedding space. We discuss KGEs in Euclidean space and then describe related work for other geometries.

Euclidean Embedding Models A large number of KGE models such as TransE (Bordes et al. 2013) and its variants (Ji et al. 2015; Lin et al. 2015; Wang et al. 2014) as well as RotatE (Sun et al. 2019) are designed using translational or rotational (Hadamard product) score functions in Euclidean space. The score and loss functions of these models optimize the embedding vectors in a way that maximise the plausibility of triples, which is measured by the distance between rotated/translated head and tail vectors. Some embedding models such as DisMult (Yang et al. 2015), ComplEx (Trouillon et al. 2016), QuatE (Zhang et al. 2019), and RESCAL (Nickel, Tresp, and Krieger 2011), including our proposed model, are designed based on element-wise multiplication of transformed head and tail. In this case, the plausibility of triples is measured based on the angle of transformed head and tail. A third category of KGE models are those designed on top of Neural Networks (NN) as score function such as ConvE (Dettmers et al. 2018) and NTN (Socher et al. 2013).

Non-Euclidean Embedding Models The aforementioned KGE models are limited to Euclidean space, which limits their ability to embed complex structures. Some recent efforts (Weber and Nickel 2018; Chami et al. 2020) inves-

tigated other spaces for embeddings of structures - often simpler structures than KGs. For example, the hyperbolic space has been extensively studied in scale-free networks. In recent work, learning continuous hierarchies from unstructured similarity scores using the Lorentz model was investigated (Nickel and Kiela 2018). In (Balazevic, Allen, and Hospedales 2019a), an embedding model dubbed MuRP is proposed that embeds multi-relational KGs on a Poincaré ball (Ji et al. 2016). MuRP only focuses on resolving the problem of embedding on KGs with multiple simultaneous hierarchies. Overall, while the advantages of projective geometry are eminent in a wide variety of application domains, including computer vision and robotics, to our knowledge no investigation has focused on it within the context of knowledge graph embeddings.

Method

Our method 5★E inherits the five main pillars of projective transformation, namely translation, rotation, homothety, inversion and reflection. The transformations are performed in the following steps: (1) *element-wise stereographic projection* to map the head entity from a complex plane into a point on a Riemann Sphere; (2) *relation-specific transformation* to move the Riemann Sphere into a new position and/or direction; (3) *stereographic projection* to project the mapped head from the Riemann Sphere to a complex plane (1-3 in Equations 15 and 12), (4) *selection of complex inner product* between the transformed head and the tail (Equation 6).

Model Formulation

Embedding on a Complex Projective Line Given a triple (h, r, t) , the head and tail entities $h, t \in \mathcal{E}$ are embedded into a d dimensional complex projective line i.e. $\mathbf{h}, \mathbf{t} \in \mathbb{C}\mathbb{P}^d$. A relation $r \in \mathcal{R}$ is embedded into a d dimensional vector \mathbf{r} where each element is a 2×2 matrix. \mathbf{r} contains four complex vectors $\mathbf{r}_a, \mathbf{r}_b, \mathbf{r}_c$ and $\mathbf{r}_d \in \mathbb{C}^d$. With $\mathbf{r}_{ai}, \mathbf{r}_{bi}, \mathbf{r}_{ci}, \mathbf{r}_{di}, \mathbf{h}_i, \mathbf{t}_i$, we refer to the i th element of $\mathbf{r}_a, \mathbf{r}_b, \mathbf{r}_c, \mathbf{r}_d, \mathbf{h}, \mathbf{t}$ respectively.

Relation-specific Transformation Based on preliminaries a projective transformation on a complex projective line has an equivalent transformation on the Riemann Sphere. Therefore, we use both of these perspectives in our model formulation.

Möbius Representation of Transformation: We use a relation-specific Möbius transformation to map the head entity $(\mathbf{h}_{r,i})$ from a source to a target complex plane $(\hat{\mathbb{C}})$. The

transformation is performed using stereographic projection and transformation (ϑ) on/from the Riemann Sphere. To do so, we compute \mathbf{h}_{r_i} to specify the element-wise transformation:

$$\mathbf{h}_{r_i} = g_{r_i}(\mathbf{h}_i) = \vartheta(\mathbf{h}_i, \mathbf{r}_i) = \frac{\mathbf{r}_{ai}\mathbf{h}_i + \mathbf{r}_{bi}}{\mathbf{r}_{ci}\mathbf{h}_i + \mathbf{r}_{di}}, \quad (4)$$

$$\mathbf{r}_{ai}\mathbf{r}_{di} - \mathbf{r}_{bi}\mathbf{r}_{ci} \neq 0, i = 1, \dots, d.$$

This results in the relation-specific transformed head entity $\mathbf{h}_r = [\mathbf{h}_{r_1}, \dots, \mathbf{h}_{r_d}]$.

Projective Representation of Transformation: Using homogeneous coordinates, we can also represent Equation 15 as a projective transformation:

$$\mathbf{h}_{r_i} \doteq [g_r(\mathbf{h}_i), 1]^T = \mathfrak{S}_{r_i}[\mathbf{h}_i, 1]^T, i = 1, \dots, d, \quad (5)$$

where \doteq shows dehomogenization, $\mathfrak{S}_{r_i} = \begin{bmatrix} \mathbf{r}_{ai} & \mathbf{r}_{bi} \\ \mathbf{r}_{ci} & \mathbf{r}_{di} \end{bmatrix}$ and $\det \mathfrak{S}_{r_i} \neq 0$ i.e. \mathfrak{S}_{r_i} s are invertible. The matrix representation of Equation 12 is $\mathbf{h}_r = \mathbf{R}_r[\mathbf{h} : \mathbf{1}]$, where $\mathbf{R}_r = \text{diag}(\mathfrak{S}_{r_1} \dots, \mathfrak{S}_{r_d})$ and $\mathbf{1}$ is a vector with all the elements being 1.

Score Function The correctness of triples in a KG is the similarity $(\mathbf{h}_r, \mathbf{t})$ between the relation-specific transformed head \mathbf{h}_r and tail \mathbf{t} . The model aims to minimize the angle between \mathbf{h}_r and tail \mathbf{t} , i.e. their product $(\langle \mathbf{h}_r, \mathbf{t} \rangle)$ is maximized for positive triples. For sampled negative triples, it is conversely minimized. Overall, the score function for $5^\star E$ is

$$f(h, r, t) = \text{Re}(\langle \mathbf{h}_r, \bar{\mathbf{t}} \rangle), \quad (6)$$

where $\text{Re}(x)$ is the real part of the complex number x .

Theoretical Analysis

We first show that $5^\star E$ covers the five transformations. We then discuss the capability of $5^\star E$ in preserving graph structures. We also prove $5^\star E$ is fully expressive and subsumes various state-of-the-art KGE models.

Möbius – Composition of Transformations The Möbius transformation in Equation 15 is a composition of a series of five subsequent transformations ϑ_1, ϑ_2 (two transformations in one), ϑ_3 and ϑ_4 as shown in (Kisil 2012): $\mathbf{h}_{r_i} = \vartheta(\mathbf{h}_i, \mathbf{r}_i) = \vartheta_4 \circ \vartheta_3 \circ \vartheta_2 \circ \vartheta_1(\mathbf{h}_i, \mathbf{r}_i)$, where $\vartheta_1(\mathbf{x}, \mathbf{r}_i) = \mathbf{x} + \frac{\mathbf{r}_{di}}{\mathbf{r}_{ci}}$ (translation by $\frac{\mathbf{r}_{di}}{\mathbf{r}_{ci}}$), $\vartheta_2(\mathbf{x}) = \frac{1}{\mathbf{x}}$ (inversion and reflection w.r.t. real axis), $\vartheta_3(\mathbf{x}, \mathbf{r}_i) = \frac{\mathbf{r}_{bi}\mathbf{r}_{ci} - \mathbf{r}_{ai}\mathbf{r}_{di}}{\mathbf{r}_{ci}^2} \mathbf{x}$ (homothety and rotation) and $\vartheta_4(\mathbf{x}, \mathbf{r}_i) = \mathbf{x} + \frac{\mathbf{r}_{ai}}{\mathbf{r}_{ci}}$ (translation by $\frac{\mathbf{r}_{ai}}{\mathbf{r}_{ci}}$). This shows that $5^\star E$ is capable of performing 5 transformations simultaneously.

Capturing Structures in a Neighborhood $5^\star E$ inherits various important properties of projective transformation as well as Möbius transformations. Because the projective linear group $PGL(2, \mathbb{C})$ is isomorphic to the Möbius group, i.e., $PGL(2, \mathbb{C}) \cong \text{Aut}(\hat{\mathbb{C}})$ (Kisil 2012), the properties which are mentioned for Equation 12 are also valid for Equation 15. We investigate the inherited properties of $5^\star E$ on *clustering similar nodes of a neighborhood* and *Capturing Sub-graph Structures*.

Clustering. The similarity of nodes in a KG is local, i.e. nodes within a close neighborhood are more likely to be

semantically similar (Faerman et al. 2018; Hamilton, Ying, and Leskovec 2017) than nodes at a higher distance. A projective transformation is a bijective conformal mapping, i.e. it preserves angle locally but not necessarily the length. It also preserves orientation after mapping (Kisil 2012). Therefore, $5^\star E$ is capable of capturing similarity by preserving angle locally via a relation-specific transformation.

Furthermore, the map $\pi : GL(2, \mathbb{C}) \rightarrow \text{Aut}(\hat{\mathbb{C}})$ is a group homomorphism, where $GL(2, \mathbb{C})$ is a generalized linear group, which transfers the matrix \mathfrak{S} into a Möbius transformation ϑ . If $\det \mathfrak{S} = 1$, then $\pi : SL(2, \mathbb{C}) \rightarrow \text{Aut}(\hat{\mathbb{C}})$ becomes limited to only perform a mapping from the special linear group $SL(2, \mathbb{C})$ to a Möbius group that preserves volume and orientation.

In the context of KGs, after a relation-specific transformation (Equation 12 or equivalently Equation 15) of nodes in the head position to nodes in tail position, the relative distance of nodes can be preserved. From this ability, we expect that $5^\star E$ is able to propagate the structural similarity from one group of nodes to another.

Capturing Sub-graph Structures. Going beyond $SL(2, \mathbb{C})$ by changing the determinant to $\det \mathfrak{S} \neq 1$, the volume and orientation of the graph sub-structures are changed after transformation. Therefore, $5^\star E$ is more flexible than current KGEs as those are not able to change volume and orientation of subgraphs. This is visible in Figure 1 when the graph includes a group of nodes in a path structure besides another group of nodes with a loop structure. In the vector space, other KGEs encounter a problem in preserving this type of graph structure due to the limited transformation abilities (not supporting inversion and reflection), whereas they work fine for homogeneous structures (e.g. only lines or only circles). In contrast to this, $5^\star E$ is capable of transforming heterogeneous structures due to the characteristics of a projective transformation (Kisil 2012).

Subsumption of Other Models We show that $5^\star E$ subsumes other models and inherits their favorable characteristics in learning various graph patterns.

Definition 1. A model M_1 subsumes M_2 when any scoring over triples of a KG measured by model M_2 can also be obtained by M_1 (Wang, Gemulla, and Li 2018).

Proposition 1. $5^\star E$ with variants of its score function subsumes *DistMult*, *pRotatE*, *RotatE*, *TransE* and *Complex*. Specifically, $5^\star E$ subsumes *DistMult*, *Complex* and *pRotatE* with $f(h, r, t) = \text{Re}(\langle \mathbf{h}_r, \bar{\mathbf{t}} \rangle)$ and subsumes *RotatE* and *TransE* with score function $f(h, r, t) = -\|\mathbf{h}_r - \mathbf{t}\|$ (changed inner product to distance).

Definition 2 (from (Kazemi and Poole 2018)). A model M is *fully expressive* if there exist assignments to the embeddings of the entities and relations, that accurately separate correct triples for any given ground truth.

Corollary 1. The $5^\star E$ model is fully expressive.

Inference of Patterns For relations which exhibit patterns in the form of *premise* \rightarrow *conclusion*, where *premise* can be a conjunction of several triples, a model is said to be able to infer those if the implication holds for the score function, i.e. if the score of all triples in the premise is positive then

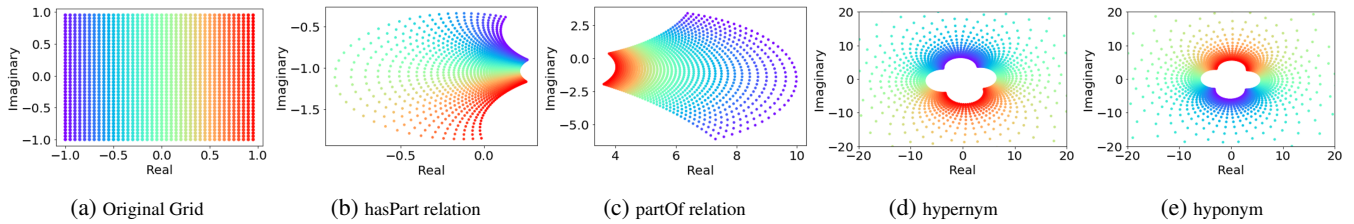


Figure 3: Learned 5★E embeddings for a selected relations in WordNet. (b)-(e) show how the lines in (a) are transformed for a particular dimension (the 12th dimension in this case) of the embedding of the mentioned relations.

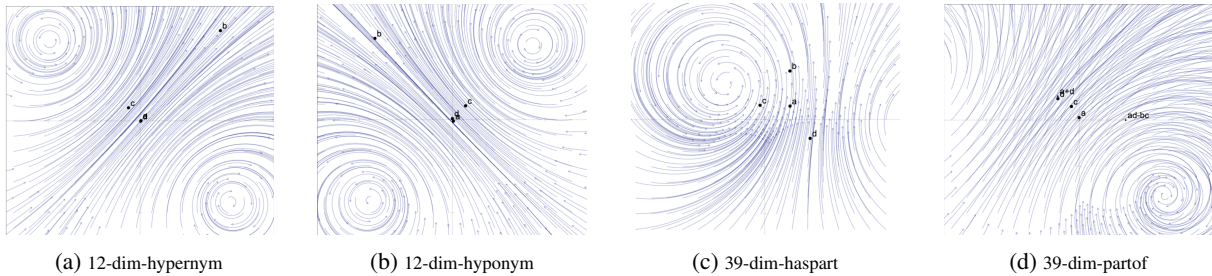


Figure 4: Embeddings for different relations using the same dimension.

the score for the conclusion must be positive. 5★E is able to infer reflexive, symmetric, inverse relation patterns as well as composition.

Proposition 2. Let $r_1, r_2, r_3 \in \mathcal{R}$ be relations and r_3 (e.g. *UncleOf*) be a composition of r_1 (e.g. *BrotherOf*) and r_2 (e.g. *FatherOf*). 5★E infers composition with $\mathfrak{S}_{r_1} \mathfrak{S}_{r_2} = \mathfrak{S}_{r_3}$.

Proposition 3. Let $r_1 \in \mathcal{R}$ be the inverse of $r_2 \in \mathcal{R}$. 5★E infers this pattern with $\mathfrak{S}_{r_1} = \mathfrak{S}_{r_2}^{-1}$.

Proposition 4. Let $r \in \mathcal{R}$ be symmetric. 5★E infers the symmetric pattern if $\mathfrak{S}_r = \mathfrak{S}_r^{-1}$.

Proposition 5. Let $r \in \mathcal{R}$ be a reflexive relation. In dimension d , 5★E infers reflexive patterns with $O(2^d)$ distinct representations of entities if the fixed points are non-identical.

TransE only infers composition and inverse patterns. RotatE is capable of inferring more patterns but is not fully expressive. ComplEx infers these patterns and is fully expressive. However, it has less flexibility than our model in learning complex structures due to using only rotation and homothety. Therefore, it is only capable of preserving homogeneous structures (see Figure 5).

Experiments and Results

Experimental Setup Following the best practices of evaluations for embedding models, we consider the most-used metrics (Mean) Reciprocal Rank (MRR) and Hits@n ($n = 1, 3, 10$). We evaluated our model on four widely used benchmark datasets namely FB15k-237 (Toutanova and Chen 2015), WN18RR (Dettmers et al. 2018), and NELL (four different versions as NELL-995-h25, NELL-995-h50, NELL-995-h75 and NELL-995-h100) (Xiong,

Hoang, and Wang 2017; Balazevic, Allen, and Hospedales 2019a). The FB15k-237 and WN18RR datasets both include several relational patterns such as composition (e.g. *awardnominee/.../nominatedfor*), symmetry (e.g. *derivationally_related_form* in WN18RR), and anti-symmetry (e.g. *has_part* in WN18RR). The WN18RR dataset includes hierarchical relations such as *hypernym* and *has_part*, which are typical examples for shaping a path structure, and relations such as *also_see*, *similar_to*, which are candidates for loop structures. The different variants of the NELL dataset include several relations that contain loops (*hassibling*, *competeswith*, *synonymfor*) as well as relations forming hierarchical paths (*subpartof*).

We compare the best performing models namely *TransE* (Bordes et al. 2013), *RotatE* (Sun et al. 2019), *TuckEr* (Balazevic, Allen, and Hospedales 2019b), *ComplEx* (Trouillon et al. 2016), *QuatE* (Zhang et al. 2019), *MuRP* (Balazevic, Allen, and Hospedales 2019a), *ConvE* (Dettmers et al. 2018) and *SimplE* (Kazemi and Poole 2018). Our model is implemented in Pytorch¹ and the code is available online². Similar to QuatE and ComplEx, we developed our model on top of a standard framework (Lacroix, Usunier, and Obozinski 2018), applied 1-N scoring loss with N3 regularization, and added reverse counterparts of each triple to the train set.

Results. The results of comparing 5★E to other models on FB15k-237 and WN18RR are shown in Table 1 ($d = 100$ and 500) and on NELL in Table 2 ($d = 100$ and 200). Our model outperforms all other models across all metrics on WN18RR, which is a dataset with many hierarchical relations as well as relations forming loops such as *similar - to*. Although

¹<https://pytorch.org/>

²<https://bit.ly/2NXplO1>

Model	FB15k237				WN18RR			
	MRR	Hits@1	Hits@3	Hits@10	MRR	Hits@1	Hits@3	Hits@10
TransE	0.29	-	-	0.47	0.23	-	-	0.50
RotatE	0.34	0.24	0.38	0.53	0.48	0.43	0.49	0.57
TuckEr	0.36	0.27	0.39	0.54	0.47	0.44	0.48	0.53
ComplEx	0.36	0.27	0.40	0.56	0.49	0.44	0.50	0.58
QuatE	0.37	0.27	0.40	0.56	0.48	0.44	0.50	0.57
ConvE	0.33	0.24	0.36	0.50	0.43	0.40	0.44	0.52
MuRP	0.34	0.24	0.37	0.52	0.48	0.44	0.50	0.57
5★E $d = 500$	0.37	0.28	0.40	0.56	0.50	0.45	0.51	0.59
5★E $d = 100$	0.35	0.26	0.38	0.53	0.47	0.41	0.50	0.58

Table 1: Link prediction results on d FB15k-237, and WN18RR. The Results of TransE, QuatE, RotatE, and ConvE are taken from (Zhang et al. 2019), TuckER from (Balazevic, Allen, and Hospedales 2019b) and MuRP from (Balazevic, Allen, and Hospedales 2019a), and ComplEx has been experimented.

Model	NELL-995-h100				NELL-995-h75			
	MRR	Hits@1	Hits@3	Hits@10	MRR	Hits@1	Hits@3	Hits@10
MuRE	0.36	0.27	0.40	0.53	0.36	0.27	0.40	0.53
MuRP	0.36	0.27	0.40	0.53	0.36	0.28	0.40	0.52
ComplEx	0.35	0.27	0.40	0.52	0.35	0.27	0.39	0.51
QuatE	0.35	0.26	0.40	0.53	0.36	0.27	0.41	0.52
5★E $d = 200$	0.37	0.28	0.42	0.54	0.37	0.28	0.41	0.53
5★E $d = 100$	0.36	0.28	0.40	0.53	0.36	0.27	0.39	0.53
Model	NELL-995-h50				NELL-995-h25			
	MRR	Hits@1	Hits@3	Hits@10	MRR	Hits@1	Hits@3	Hits@10
MuRE	0.37	0.28	0.42	0.54	0.37	0.29	0.40	0.52
MuRP	0.37	0.28	0.42	0.54	0.36	0.28	0.40	0.51
ComplEx	0.37	0.29	0.41	0.52	0.37	0.30	0.40	0.51
QuatE	0.36	0.27	0.40	0.53	0.36	0.28	0.40	0.51
5★E $d = 200$	0.38	0.30	0.43	0.54	0.39	0.31	0.43	0.53
5★E $d = 100$	0.38	0.29	0.43	0.54	0.37	0.30	0.41	0.52

Table 2: Link prediction results on KGs with various percentages of hierarchical relations including NELL-995-h25 (25% hierarchical relation) and NELL-995-h50 (50%) as well as NELL-995-h75 (75%) and NELL-995-h100 (100%). The results for ComplEx, QuatE, and 5★E are from own experiments - all others are taken from their original works.

MuRP is specifically designed for hierarchical data, 5★E still achieves a better performance. Generally, we can observe that 5★E obtains competitive results with a low dimension ($d = 100$) on WN18RR for the Hits@3 and Hits@10 metrics.

The evaluation shows that rotation-based models (RotatE, QuatE, and ComplEx) obtain state-of-the-art results on the FB15k-237 dataset (with fewer hierarchical paths than WN18RR). Our model, which covers rotation and transformation, obtains similar results to those models. On this dataset, there is no evident benefit of supporting further transformations. We additionally used different versions of the NELL dataset, which are specifically designed to have a particular percentage of hierarchical relations. 5★E outperforms other models in all NELL dataset versions.

Overall, the competitive results of 5★E show that additional transformations have a positive effect for the link prediction task. They also indicate that the additional transformations do not lead to over-fitting problems compared to

single-transformation models (or at least the positive effects outweigh potential overfitting).

Learned Transformation Types Each relation in the KG is represented as d projective transformations in 5★E (one projective transformation per dimension). Figure 3 shows the transformation types learned by 5★E for the relations of WordNet. The original plain view of the grid is given in sub-graph (a) for comparisons of the changes after the transformations, and (b) to (e) show specific relations in WordNet. The mapping of the *lines* (same-color points) in the original grid to *circle or curve* in sub-graph (b)-(e) indicates an application of an inversion transformation for relation-specific transformations (*hasPart*, *partOf*, *hypernym* and *hyponym*). By comparing the direction of the lines with the same color (e.g., red) in the original grid and in all examples of the transformed grids, we can observe that the learned transformations cover rotation (*hypernym*, and *hyponym*). We can also interpret the results for the *hasPart* relation as counter-clockwise

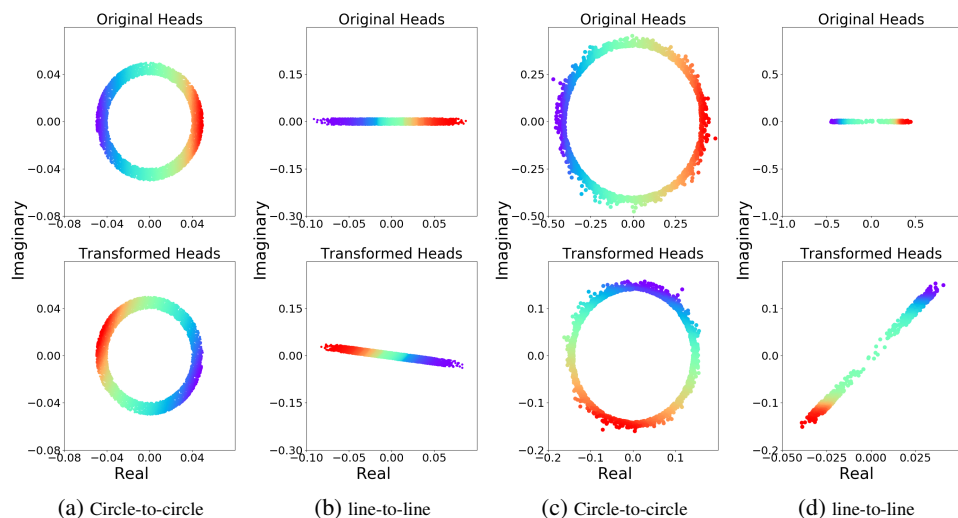


Figure 5: Types of transformations that RotatE (a,b) and ComplEx (c,d) learned on relation "hypernym" in WordNet. Each pair of images visualises one dimension of the relation embedding. The top images show the embeddings of head entities of this relation in the KG at this dimension. Each entity embedding is visualised as a colored dot. The bottom images show the results of applying the relation specific transformation (the entity colors are preserved).

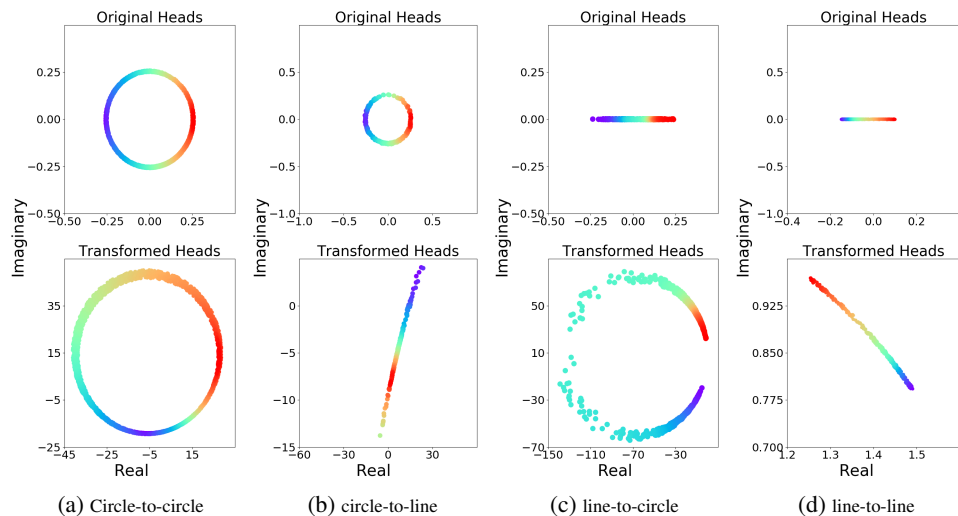


Figure 6: Types of transformations that 5★E learned on relation "hypernym" in WordNet. Each pair of images visualises one dimension of the relation embedding. The top images show the embeddings of head entities of this relation in the KG at this dimension. Each entity embedding is visualised as a colored dot. The bottom images show the results of applying the relation specific transformation (the entity colors are preserved).

rotation and then reflection w.r.t. the real axis. In sub-graph (b), there is a movement in the real and imaginary axis of the grid towards down and slightly right for the *hasPart* relation, which represents translation. However, this is not the case for the *hypernym* relation. Semantically, the pairs (*hypernym*, *hyponym*) and (*hasPart partOf*) form inverse patterns (see Corollary 3). We see that the transformed grids of *hypernym* and *hyponym* are different only w.r.t. rotation. The scale is not changed, so the determinants of the two projective matrices are 1 (no homothety). For the *hasPart* and *partOf* grids, we can observe that the scale is changed, so the determinant of

those two projection matrices should not be equal to one. This shows that both of those transformations cover *homothety*.

Moreover, each of the five transformation functions performed in Figure 9 are also learned by 5★E which confirms the flexibility of the model as well as diversity in density/sparsity of flows. Figure 15 shows the analysis on the example of *hyponym* and *hypernym* as well as *hasPart* and *partOf* relations which are mutually inverse of each other. Based on their inverse characteristic, we have $\mathfrak{S}_{Hypernym} = \mathfrak{S}_{Hyponym}^{-1}$. As the representing matrices (\mathfrak{S}) are normalized, their determinant is equal to one. Consequently,

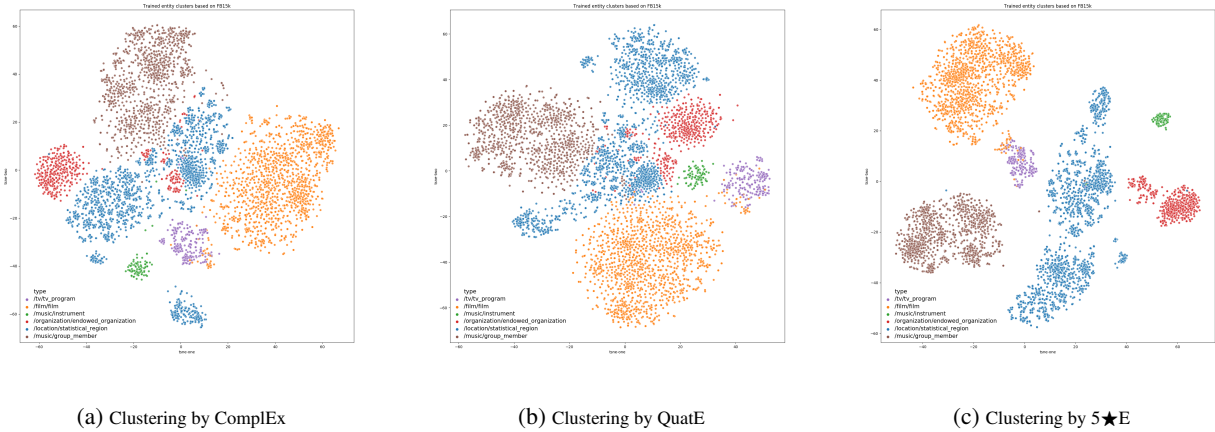


Figure 7: Comparison of clustering results between ComplEx, QuatE, and 5★E (left to right). Each color shows a class of entities and each point is one instance entity of the corresponding class.

we have $tr(\mathfrak{S}_{Hypernym}) = tr(\mathfrak{S}_{Hyponym}^{-1})$ when the learned transformation function is elliptic. We conclude that in our experiments for a pair of inverse relations, the learned transformation functions are in the same category (elliptic) for the i -th element of the relation embedding. In Figure 15, sub-figures (a) and (b) illustrate that the learned functions fall into the elliptic category for the same embedding dimension ($i = 12$) of *hyponym* and *hypernym*. The difference between the embeddings for this pair of inverse relations is their rotation. The same pattern is notable for the *hasPart* and *partOf* relations in sub-figures (c) and (d) for $i = 39$. Figure 5 shows the mapping of lines and circles by other KGEs. When observing each dimension of each relation, there was not a single case where a shape has been mapped to a different one, which empirically confirms our theoretical finding that existing models can only perform homogeneous transformations. In contrast, Figure 6 shows a relation-specific mapping of line to circle and circle to line performed by 5★E model.

Entity Clustering As mentioned in theoretical analysis, our model uses a bijective conformal mapping in the projective geometry which consequently preserves angle locally. In Figure 7, we provide an evaluation for the performance of the models in terms of clustering. More precisely, Figures 10, 11 and 12 show the clustering of nodes in Freebase KG (Moon, Jones, and Samatova 2017) and illustrate comparisons to QuatE, ComplEx and 5★E. In this visualization, we can see that entities of the same type are closer in 5★E as compared to the competitors. Moreover, the distance between cluster centers in 5★E is higher than in the other models. Therefore, it is visible that 5★E provides a more suitable clustering for this dataset than other competitors.

Conclusion

In this paper, we introduce a new KGE model which operates on the complete set of projective transformations. We build the model on well researched generic mathematical foundations and showed that it subsumes other state-of-the-art

embedding models. Furthermore, we prove that the model is fully expressive. By supporting a wider range of transformations than previous models, it can embed KGs with more complex structures and supports a wide range of relational patterns. We empirically studied and visualised the effects using the example of loop and path combinations. Our experimental evaluation on six benchmark datasets using established metrics shows that the model outperforms previous approaches of knowledge graph embedding models.

Acknowledgements

We acknowledge the support of the following projects: SPEAKER (BMW FKZ 01MK20011A), JOSEPH (Fraunhofer Zukunftsstiftung), Cleopatra (GA 812997), the excellence clusters ML2R (BmBF FKZ 01 15 18038 A/B/C), MLwin (01IS18050), ScaDS.AI (IS18026A-F), TAILOR (EU GA 952215), and H2020-EU PLATOON (872592).

References

- Balazevic, I.; Allen, C.; and Hospedales, T. 2019a. Multi-relational Poincaré graph embeddings. In *Advances in Neural Information Processing Systems*, 4465–4475.
- Balazevic, I.; Allen, C.; and Hospedales, T. 2019b. TuckER: Tensor Factorization for Knowledge Graph Completion. In *EMNLP-IJCNLP Conference*, 5188–5197.
- Bollacker, K.; Evans, C.; Paritosh, P.; Sturge, T.; and Taylor, J. 2008. Freebase: a collaboratively created graph database for structuring human knowledge 1247–1250.
- Bordes, A.; Usunier, N.; Garcia-Duran, A.; Weston, J.; and Yakhnenko, O. 2013. Translating embeddings for modeling multi-relational data. In *Advances in neural information processing systems*, 2787–2795.
- Chami, I.; Wolf, A.; Juan, D.-C.; Sala, F.; Ravi, S.; and Ré, C. 2020. Low-Dimensional Hyperbolic Knowledge Graph Embeddings. In *Proceedings of the 58th Annual Meeting of the Association for Computational Linguistics*, 6901–6914.

- Dettmers, T.; Minervini, P.; Stenetorp, P.; and Riedel, S. 2018. Convolutional 2d knowledge graph embeddings. In *Thirty-Second AAAI Conference*.
- Faerman, E.; Borutta, F.; Fountoulakis, K.; and Mahoney, M. W. 2018. Lasagne: Locality and structure aware graph node embedding. In *International Conference on Web Intelligence (WI)*, 246–253. IEEE.
- Hamilton, W. L.; Ying, R.; and Leskovec, J. 2017. Representation learning on graphs: Methods and applications. *arXiv preprint arXiv:1709.05584*.
- Ji, G.; He, S.; Xu, L.; Liu, K.; and Zhao, J. 2015. Knowledge graph embedding via dynamic mapping matrix. In *Proceedings of the 53rd Annual Meeting of the Association for Computational Linguistics and the 7th International Joint Conference on Natural Language Processing (Volume 1: Long Papers)*, 687–696.
- Ji, G.; Liu, K.; He, S.; and Zhao, J. 2016. Knowledge Graph Completion with Adaptive Sparse Transfer Matrix. 985–991.
- Ji, S.; Pan, S.; Cambria, E.; Marttinen, P.; and Yu, P. S. 2020. A survey on knowledge graphs: Representation, acquisition and applications. *arXiv preprint arXiv:2002.00388*.
- Kazemi, S. M.; and Poole, D. 2018. Simple embedding for link prediction in knowledge graphs. In *Advances in neural information processing systems*, 4284–4295.
- Kisil, V. V. 2012. *Geometry of Möbius Transformations: Elliptic, Parabolic and Hyperbolic Actions of SL_2 [real Number]*. World Scientific.
- Lacroix, T.; Usunier, N.; and Obozinski, G. 2018. Canonical Tensor Decomposition for Knowledge Base Completion. In *International Conference on Machine Learning (ICML)*, 2863–2872.
- Lin, Y.; Liu, Z.; Sun, M.; Liu, Y.; and Zhu, X. 2015. Learning entity and relation embeddings for knowledge graph completion. In *Twenty-ninth AAAI conference on artificial intelligence*.
- Miller, G. A. 1995. WordNet: a lexical database for English. *Communications of the ACM* 38(11): 39–41.
- Moon, C.; Jones, P.; and Samatova, N. F. 2017. Learning entity type embeddings for knowledge graph completion. In *Proceedings of the 2017 ACM on conference on information and knowledge management*, 2215–2218.
- Nickel, M.; and Kiela, D. 2018. Learning Continuous Hierarchies in the Lorentz Model of Hyperbolic Geometry. volume 80 of *Proceedings of Machine Learning Research*, 3779–3788. PMLR.
- Nickel, M.; Tresp, V.; and Kriegel, H.-P. 2011. A Three-Way Model for Collective Learning on Multi-Relational Data. 11: 809–816.
- Richter-Gebert, J. 2011. *Perspectives on projective geometry: A guided tour through real and complex geometry*. Springer Science & Business Media.
- Salomon, D. 2007. *Transformations and projections in computer graphics*. Springer Science & Business Media.
- Socher, R.; Chen, D.; Manning, C. D.; and Ng, A. 2013. Reasoning with neural tensor networks for knowledge base completion 926–934.
- Sun, Z.; Deng, Z.-H.; Nie, J.-Y.; and Tang, J. 2019. Rotate: Knowledge graph embedding by relational rotation in complex space. *arXiv preprint arXiv:1902.10197*.
- Tim Hutton. 2020. Mobius Transforms. <https://github.com/timhutton/mobius-transforms>. Online; accessed 15 December 2020.
- Toutanova, K.; and Chen, D. 2015. Observed versus latent features for knowledge base and text inference. In *Proceedings of the 3rd Workshop on Continuous Vector Space Models and their Compositionality*, 57–66.
- Trouillon, T.; Welbl, J.; Riedel, S.; Gaussier, É.; and Bouchard, G. 2016. Complex embeddings for simple link prediction. In *International Conference on Machine Learning*, 2071–2080.
- Wang, Y.; Gemulla, R.; and Li, H. 2018. On multi-relational link prediction with bilinear models. In *Thirty-Second AAAI Conference on Artificial Intelligence*.
- Wang, Z.; Zhang, J.; Feng, J.; and Chen, Z. 2014. Knowledge graph embedding by translating on hyperplanes. In *Twenty-Eighth AAAI conference on artificial intelligence*.
- Weber, M.; and Nickel, M. 2018. Curvature and Representation Learning: Identifying Embedding Spaces for Relational Data. *NeurIPS Relational Representation Learning*.
- Xiong, W.; Hoang, T.; and Wang, W. Y. 2017. DeepPath: A Reinforcement Learning Method for Knowledge Graph Reasoning. In *EMNLP Conference*, 564–573.
- Yang, B.; Yih, W.-t.; He, X.; Gao, J.; and Deng, L. 2015. Embedding entities and relations for learning and inference in knowledge bases. In *Conference on Learning Representations (ICLR)*.
- Zhang, S.; Tay, Y.; Yao, L.; and Liu, Q. 2019. Quaternion knowledge graph embeddings. In *Advances in Neural Information Processing Systems*, 2731–2741.

Appendix

Capturing Path/loop

Here, we demonstrate an example for the cases presented in Figure 1 in the main body of the paper. We choose path/loop relation to build up our example. Assume that, we have a set of 10 different nodes which are positioned as a path (h_i where $i \dots 10$) of a specific relation (e.g. hypernym). A different set of another 10 nodes (t_i where $i \dots 10$) are connected through a relation (e.g. similar_to) in a loop structure. Our assumption is that the path structure is positioned beside a loop. The nodes in the head position are collected (e.g. through the also-see relation) to the ones in the loop position. In Figure 8, the given ranking by each embedding model for each triple is shown. Low number means a better ranking for higher plausibility of each triple, and high ranking means the chance of triple incorrectness is high. Column one shows all the possible triples which are involved in these three relations. We consider bi-directional ranking as “right hand side ranking”(RHS) and “left hand side ranking”(LHS).

The highlights to be noted are that:

- In order to preserve the shape of the loop, the triple ($t_{10}, \text{similar-to}, t_1$) should be ranked as low as possible. The problem occurs when a model gives a high rank to this triple. If this happens, the shape of the loop is transferred (wrongly) to a path.
- In order to preserve the shape of the path, the ($h_{10}, \text{similar-to}, h_1$) triple should be ranked as high as possible. The problem occurs when a model gives a low rank to this triple. If this happens, the shape of the path is transferred (wrongly) to a loop.

A perfect model should specifically learn ($t_{10}, \text{similar-to}, t_1$) as positive (rank low) in order to preserve the loop. Moreover, the model should learn ($h_{10}, \text{similar-to}, h_1$) as a negative triple with a high rank which means the path shape is preserved.

For ($t_{10}, \text{similar-to}, t_1$) triple which is expected to be ranked very low by a good KGE model, 5★E ranks this triple as low as possible (2 both for LHS and RHS), without problematically affecting the ranking of ($h_{10}, \text{similar-to}, h_1$) triple (ranked high as 19, 18). This concludes that the shape of loop and path are preserved by 5★E. However, other models completely miss-preserve the head triple of ($h_{10}, \text{similar-to}, h_1$) when they take a low rank for ($t_{10}, \text{similar-to}, t_1$). This is more visible for QuatE and RotatE. RotatE learns ($t_{10}, \text{similar-to}, t_1$) with lowest rank (1), however it also ranks ($h_{10}, \text{similar-to}, h_1$) with 1. Relatively similar behaviours is observed from QuatE. This concludes that the shape of loop is preserved by RotatE and QuatE, however it was with the cost of (wrongly) transferring path to loop as well. For TransE, a relatively high ranking is assigned to ($h_{10}, \text{similar-to}, h_1$) triple (which means the model expects this triple to be incorrect) and preserves the path, however this causes a high rank for ($t_{10}, \text{similar-to}, t_1$) as well. We see in that by using the ComplEx model, it shows a similar behaviour to TransE model. This concludes that the shape of path is preserved, however the loop part is also transferred to a path shape. This

observation in connection to Figure 1 clarifies the difficulty of other KGE models when different motifs come close in sub-graphs of a KG. Our proposed model has the potential to correctly preserve each structure separately. This power comes from the possible transformations covered in projective geometry, illustrated in Figure 9. In Table 4, the theoretical description and the validity conditions of each transformation is discussed. All transformations in each group form a subgroup which is isomorphic to the group of all matrices mentioned in the row *Iso*. Note that *tr* in the table denotes the trace of a matrix.

Vector Representation of Path/Loop by RotatE

As mentioned in the main paper, the RotatE model is not able to preserve a loop structure connected with a path from the graph representation in the vector space. To show this, without loss of generality, we investigate the example given in Figure one with a concrete scenario. Let us consider three entities (h_1, h_2, h_3) connected by the relation r_1 in a path structure i.e. (h_1, r_1, h_2), (h_2, r_1, h_3), and three other entities (t_1, t_2, t_3) connected by relation r_3 in a loop structure i.e. (t_1, r_3, t_2), (t_2, r_3, t_3), (t_3, r_3, t_1). RotatE encodes path as

$$\begin{aligned} \mathbf{h}_1 \circ \mathbf{r}_1 &\approx \mathbf{h}_2, \\ \mathbf{h}_2 \circ \mathbf{r}_1 &\approx \mathbf{h}_3, \\ \mathbf{h}_3 \circ \mathbf{r}_1 &\neq \mathbf{h}_1, \end{aligned} \quad (7)$$

and loop as

$$\begin{aligned} \mathbf{t}_1 \circ \mathbf{r}_3 &\approx \mathbf{t}_2, \\ \mathbf{t}_2 \circ \mathbf{r}_3 &\approx \mathbf{t}_3, \\ \mathbf{t}_3 \circ \mathbf{r}_3 &\approx \mathbf{t}_1. \end{aligned} \quad (8)$$

Additionally, entities of the path structure are connected to the entities of the loop structure i.e. (h_1, r_2, t_1), (h_2, r_2, t_2), (h_3, r_2, t_3), which are encoded by RotatE as

$$\begin{aligned} \mathbf{h}_1 \circ \mathbf{r}_2 &\approx \mathbf{t}_1, \\ \mathbf{h}_2 \circ \mathbf{r}_2 &\approx \mathbf{t}_2, \\ \mathbf{h}_3 \circ \mathbf{r}_2 &\approx \mathbf{t}_3. \end{aligned} \quad (9)$$

Note that the representation of relations between entities is actually a rotation in complex space when using RotatE model i.e. $\mathbf{r} = e^{i\theta}$.

After combining Equation 7 and 8, we have

$$\begin{aligned} \mathbf{h}_1 \circ \mathbf{r}_2 \circ \mathbf{r}_3 &\approx \mathbf{t}_2, \\ \mathbf{h}_2 \circ \mathbf{r}_2 \circ \mathbf{r}_3 &\approx \mathbf{t}_3, \\ \mathbf{h}_3 \circ \mathbf{r}_2 \circ \mathbf{r}_3 &\approx \mathbf{t}_1. \end{aligned} \quad (10)$$

After replacing \mathbf{t}_2 by $\mathbf{h}_2 \circ \mathbf{r}_2$ (according to equation 9) in equation 10, we have

$$\begin{aligned} \mathbf{h}_1 \circ \mathbf{r}_3 &\approx \mathbf{h}_2, \\ \mathbf{h}_2 \circ \mathbf{r}_3 &\approx \mathbf{h}_3, \\ \mathbf{h}_3 \circ \mathbf{r}_3 &\approx \mathbf{h}_1. \end{aligned} \quad (11)$$

TRIPLES	TransE		RotatE		Complex		QuatE		5*E	
	LHS	RHS	LHS	RHS	LHS	RHS	LHS	RHS	LHS	RHS
h1 hypernym h2	1	1	1	1	1	1	1	1	1	1
h2 hypernym h3	1	1	1	1	1	1	1	1	1	1
h3 hypernym h4	1	1	1	1	1	1	1	1	1	1
h4 hypernym h5	1	1	1	1	1	1	1	1	1	1
h5 hypernym h6	1	1	1	1	1	1	1	1	1	1
h6 hypernym h7	1	1	1	1	1	1	1	1	1	1
h7 hypernym h8	3	2	1	1	1	1	1	1	1	1
h8 hypernym h9	3	2	1	1	1	1	1	1	1	1
h9 hypernym h10	2	2	1	1	1	1	1	1	1	1
t1 similar_to t2	1	1	1	1	3	1	1	1	2	1
t2 similar_to t3	1	1	1	1	1	1	1	1	1	1
t3 similar_to t4	1	1	1	1	1	1	1	1	1	1
t4 similar_to t5	1	1	1	1	1	1	1	1	1	1
t5 similar_to t6	1	1	1	1	1	1	1	1	1	1
t6 similar_to t7	1	1	1	1	1	1	1	1	1	1
t7 similar_to t8	3	2	1	1	1	1	1	1	1	1
t8 similar_to t9	3	2	1	1	2	2	1	1	1	1
t9 similar_to t10	2	3	1	1	2	2	1	1	1	2
t10 similar_to t1	6	4	1	1	11	12	1	1	2	2
h1 also-see t1	2	1	1	1	1	2	1	1	1	1
h2 also-see t2	1	1	1	1	1	1	1	1	1	1
h3 also-see t3	1	1	1	1	1	1	1	1	1	1
h4 also-see t4	1	1	1	1	1	1	1	1	1	1
h5 also-see t5	1	1	1	1	1	1	1	1	1	1
h6 also-see t6	1	1	1	1	1	1	1	1	1	1
h7 also-see t7	1	1	1	1	1	1	1	1	1	1
h8 also-see t8	1	1	1	1	1	2	1	1	1	1
h9 also-see t9	1	1	1	1	1	2	1	1	1	1
h10 also-see t10	1	1	1	1	1	2	1	1	1	1
h10 hypernym h1 (NEGATIVE)	6	10	1	1	14	13	2	4	19	18

Should be ranked low to preserve loop
→

Should be ranked high to preserve path
→

Figure 8: Rankings of sample triples in loop (t_i where $i \dots 10$) and path (h_i where $i \dots 10$) shapes by different models.

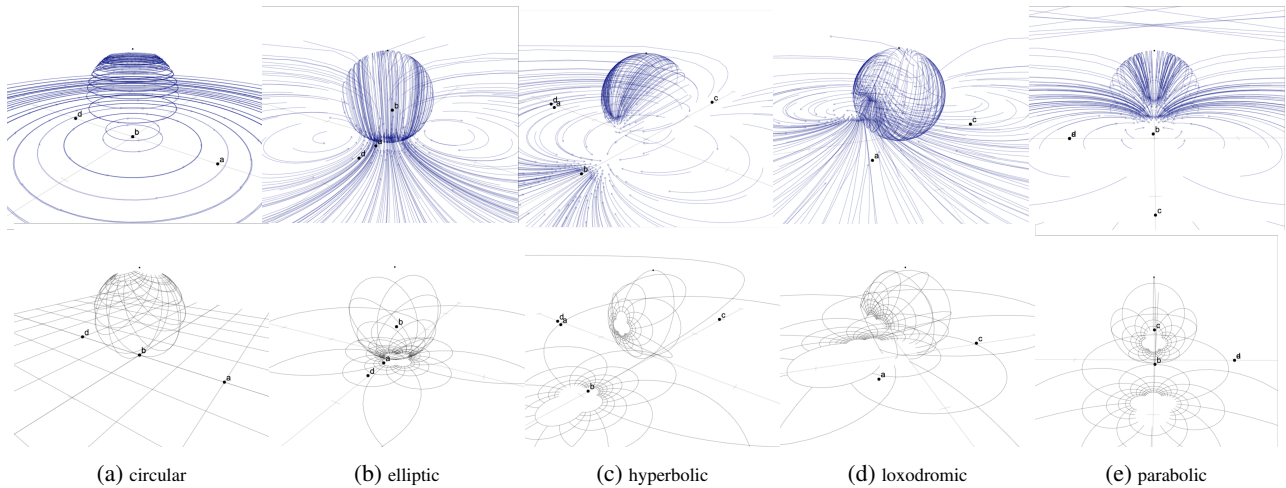


Figure 9: Default transformation functions with Riemann Sphere (first row) and the Möbius shape for each transformation after projection on a complex plane (second row) are shown.

Comparing equation 11 and 7, we have $\mathbf{r}_1 = \mathbf{r}_3$. Therefore, $\mathbf{h}_3 \circ \mathbf{r}_3 \approx \mathbf{h}_1$ and $\mathbf{h}_3 \circ \mathbf{r}_1 \neq \mathbf{h}_1$ should be held simultaneously which is in contradiction with $\mathbf{r}_1 = \mathbf{r}_3$. Based on the above-mentioned results, RotatE cannot encode loop connected with path in the vector space and either loop becomes path or path becomes loop. Similarly, we prove that other models such as QuatE (rotation in Quaternion space) and ComplEx (rotation in complex space together with homothety) also face issues when transforming a path beside a loop structure. In Table 3, we show the capability of KGEs in preserving different transformations. Correctly learning of one of these two triples, scarifies the other.

	Tra.	Rot.	Hom.	Inv.	Ref.
TransE	★	☆	☆	☆	☆
RotatE	☆	★	☆	☆	☆
ComplEx	☆	★	★	☆	☆
QuatE	☆	★	☆	☆	☆
5★E	★	★	★	★	★

Table 3: Supported Transformations by KGE Models.

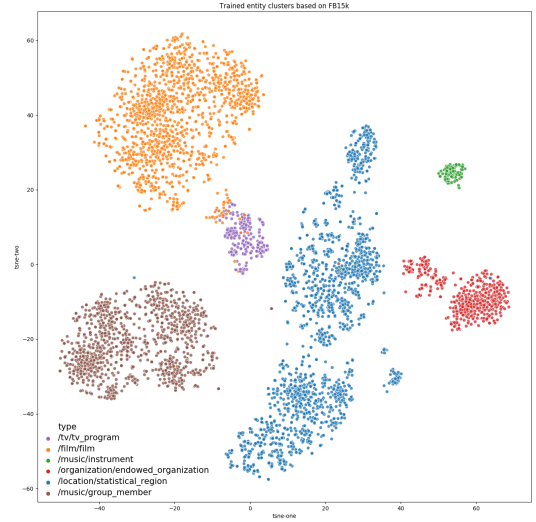


Figure 11: Clustering by 5★E

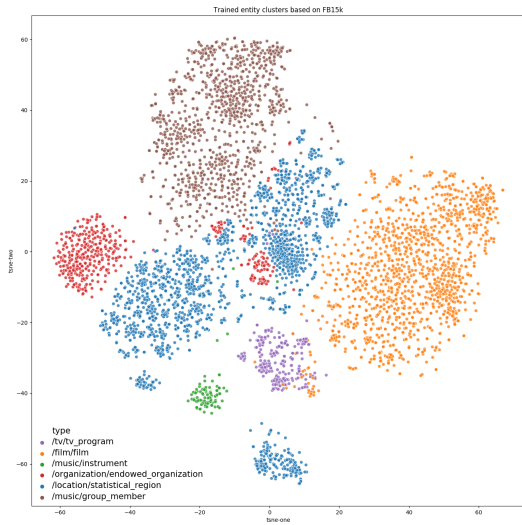


Figure 10: Clustering by ComplEx

Entity Clustering

As mentioned in the paper, our model uses bijective conformal mapping in the projective geometry which consequently preserves angle locally but not necessarily the length of motifs. Such characteristic is consistent with the nature of KGs where similarity of nodes in the graph is local i.e. nodes within a close neighborhood are more likely to be semantically similar than nodes at a higher distance. Figures 10, 11 and 12 show the clustering results of each model of QuatE, ComplEx and 5★E. According to this visualizations, 5★E puts entities of the same type more closer (lower variance)

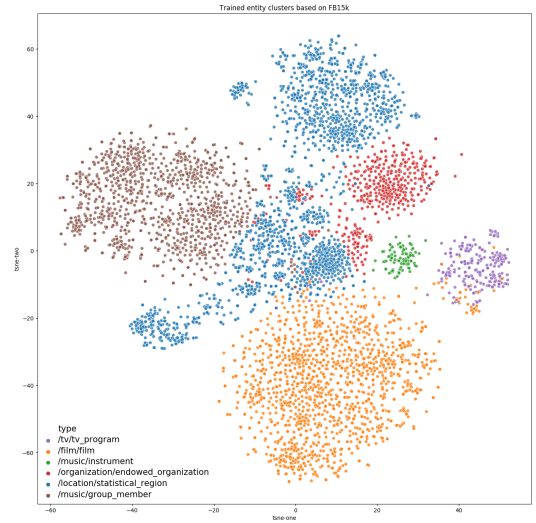


Figure 12: Clustering

than other competitors. Moreover, the distance between center of clusters in 5★E is bigger than other models. Therefore, it is visible that 5★E provides a more accurate clustering than other competitors.

Experiments On FB15K and WN18

In Table 5, the results of experimenting 5★E on FB15K and WN18 are compared to other models. In WN18, 5★E outperforms all the models in all the metrics expect Hits@10 where 0.96 is achieved by RotatE, TuckEr, QuatE, and ConvE as well as 5★E. On the FB15k dataset, we observe that 5★E outperforms TransE, RotatE, TuckEr, ComplEx, Simple, and ConvE on FB15K. 5★E and QuatE achieve a very competi-

Function	Parabolic	Circular	Elliptic	Hyperbolic	Loxodromic
Condition	$tr\mathfrak{S}^2 = 4$ ($\Delta = 0$)	$tr\mathfrak{S}^2 = 0$ ($\Delta = 0$)	$0 < tr\mathfrak{S}^2 < 4$ ($\Delta < 0$)	$tr\mathfrak{S}^2 > 4$ ($\Delta > 0$)	$tr\mathfrak{S}^2 \notin [0, 4]$
Isomorphic	$\begin{bmatrix} 1 & a \\ 0 & 1 \end{bmatrix}$	$\begin{bmatrix} i & 0 \\ 0 & -i \end{bmatrix}$	$\begin{bmatrix} e^{i\theta/2} & 0 \\ 0 & e^{-i\theta/2} \end{bmatrix}$	$\begin{bmatrix} e^{\theta/2} & 0 \\ 0 & e^{-\theta/2} \end{bmatrix}$	$\begin{bmatrix} k & 0 \\ 0 & \frac{1}{k} \end{bmatrix}$

Table 4: Types of Möbius transformations and their conditions.

Table 5: Link prediction results on WN18 and WN18RR as well as FB15k and FB15k-237.

Model	WN18				FB15k			
	MRR	Hits@1	Hits@3	Hits@10	MRR	Hits@1	Hits@3	Hits@10
TransE	0.49	0.11	0.89	0.94	0.46	0.30	0.58	0.75
RotatE	0.95	0.94	0.95	0.96	0.70	0.58	0.79	0.87
TuckEr	0.95	0.95	0.95	0.96	0.79	0.74	0.83	0.89
ComplEx	0.94	0.94	0.94	0.94	0.69	0.60	0.76	0.84
QuatE	0.95	0.94	0.95	0.96	0.83	0.80	0.86	0.90
Simple	0.94	0.94	0.94	0.95	0.73	0.66	0.77	0.84
ConvE	0.94	0.93	0.95	0.96	0.66	0.56	0.72	0.83
5★E $d=500$	0.96	0.96	0.96	0.96	0.84	0.78	0.86	0.90
5★E $d=100$	0.95	0.95	0.95	0.96	0.73	0.66	0.78	0.86

tive results in most of the cases. In MRR, our model performs slightly better, and in Hits@1, QuatE is better.

Learned Embedding: Entity Level

One of the main advantage of 5★E lies in its ability to map a line to a circle after a relation-specific transformation of the head. This means that for a given relation, e.g., *hypernym*, if the embeddings of the entities in the head position form a line, each of the transformed heads are either forming a line or a circle. Consequently, according to the formula $\mathbf{h}_{ri} = g_r(\mathbf{h}_i) = \mathbf{t}_i, i = 1, \dots, d$, the conjugated tails should also represent a shape which is close to the corresponding transformed head. In this way, 5★E captures different structural motifs of different groups of nodes. The Figures 14 and 13 illustrate the state of each relation in different dimensions with regard to their original head, transformed head, and conjugated tail. Figure 14 depicts transformations in four different dimensions for the *hypernym* relation where the line shows head entities which are located on a line and the transformed heads start to develop in the shape of a circle. Given a fixed relation r (e.g., *hypernym*), the similarity between all the transformed heads (which form a line or a circle) and the conjugated tails (similarly form a line or a circle) shows that the triples are considered positive in the vector space i.e. $g_r(\mathbf{h}_{ij}) = \mathbf{t}_{ij}, i = 1, \dots, d, j = 1, \dots, n$ where n refers to the number of entities in the head/tail position. h_{ij} refers to the i th dimension of embeddings for j th head entity. In one dimension, all the heads in Figure 13 form a line which are after transformation form a circle. Note that in each dimension (i th dimension), 5★E learns different transformation functions. Each entity in head is shown as a point. Therefore, by taking different dimensions, the shape of the transformations changes per relation.

Learned Embedding: Relation Level

The two relations *hyponym* and *hypernym* are inverse of each other. Therefore, we have $\mathfrak{S}_{Hypernym} = \mathfrak{S}_{Hyponym}^{-1}$. As these representing matrices (\mathfrak{S}) are normalized, their determinant is equal to one. Consequently, we have $tr(\mathfrak{S}_{Hypernym}) = tr(\mathfrak{S}_{Hyponym}^{-1})$ when the learned transformation function is elliptic. We conclude that for a pair of inverse relations, the learned transformation functions are in the same category (elliptic) for the i th element of the relation embedding. Figure 15, sub-figure (a) and (b) illustrate that the learned functions fall into the elliptic category for the same embedding dimension ($i = 12$) of *hyponym* and *hypernym*. The difference between the embeddings for this pair of inverse relations is their rotation. The same pattern is notable for *hasPart* and *partOf* relations in sub-figure (c) and (d) on $i = 39$.

Construction Steps of Transformations

In Figure 16 we show the learned 5★E embeddings for *hasType* relations in different epochs ranging from 0 to 49 (the stabilized epoch for this relation). The figure illustrates the gradual development of the Möbius shape over different epochs.

Experimental Setup

- Evaluation Metrics and Statistics of Standard Benchmarks** FB15K is a standard benchmark created from the original FreeBase KG (Bollacker et al. 2008). FB15K-237 (Toutanova and Chen 2015) is a sub-version of FB15K in which the inverse relations have been removed. WN18 (Bordes et al. 2013) is a lexical database with hierarchical collection for the English language that was derived from the original WordNet dataset (Miller 1995). The main relation patterns in this dataset are symmetry antisymmetry and inversion. WN18RR is a sub-version of

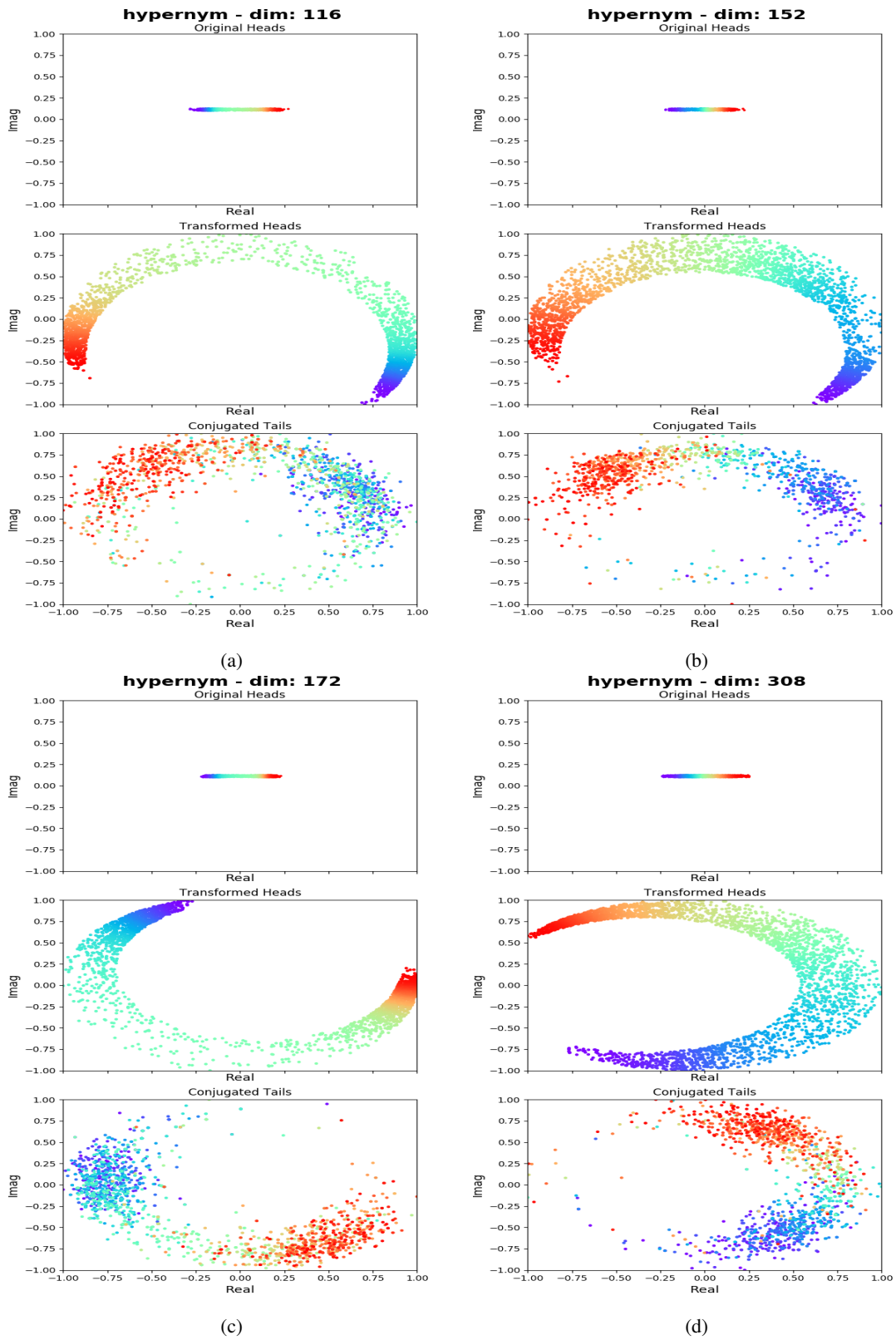


Figure 13: Learned embeddings of entities connected by the hypernym relation.

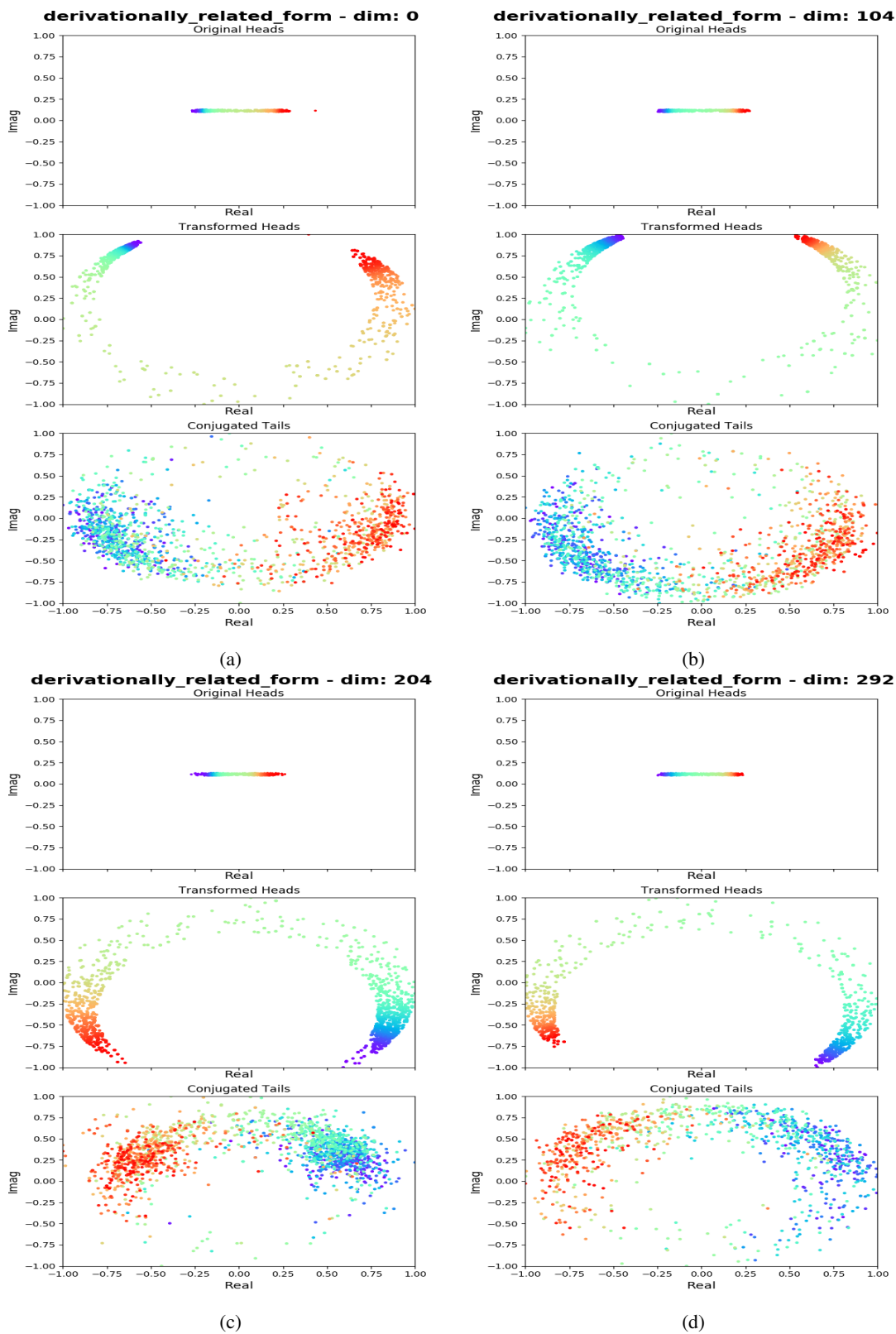


Figure 14: Learned embeddings of entities connected by the derivationally-related-form relation.

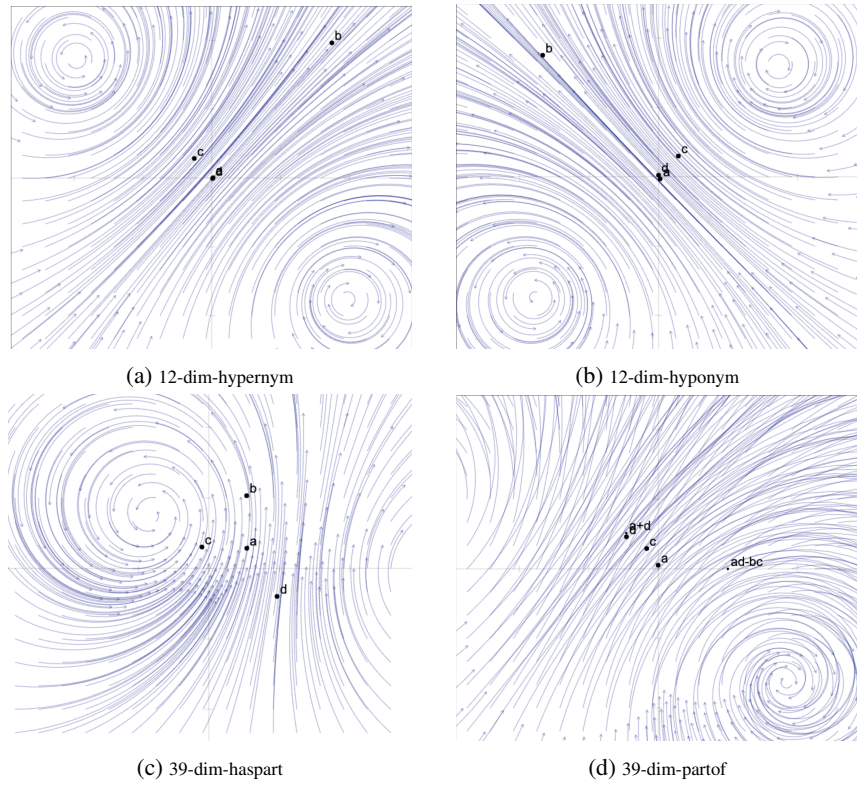


Figure 15: Embeddings for different relations using the same dimension.

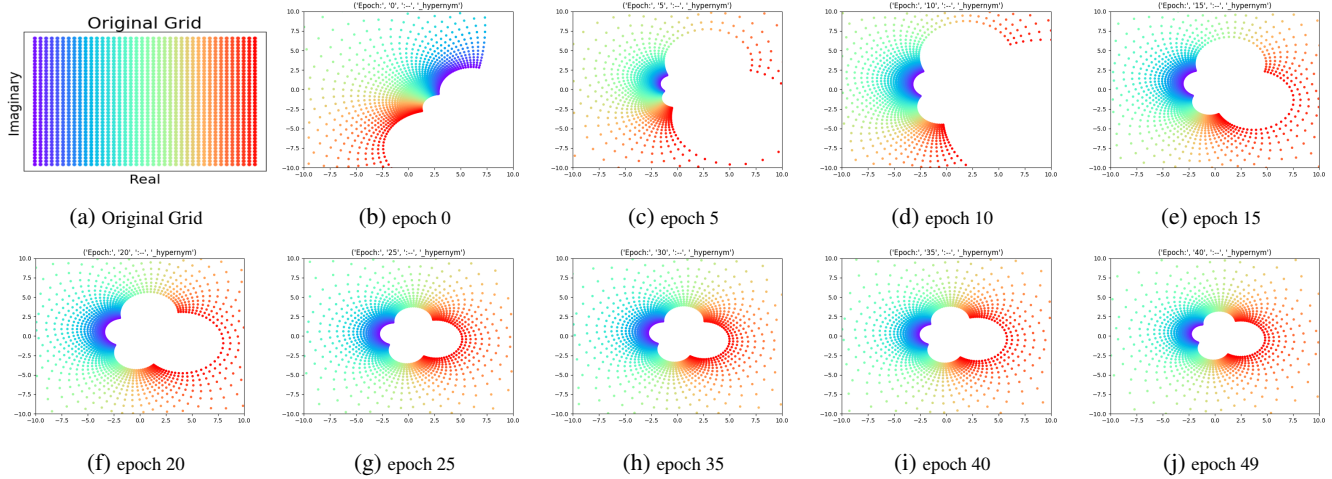


Figure 16: Learned 5★E embeddings for hasType relations in different epochs.

WN18 for which the inverse relations are omitted. We also considered four different versions of the NELL dataset in our evaluations. In Table 6, we represent the statistics of each corresponding dataset.

- Hyperparameter Search** Generally, the range of embedding dimensions were fixed to $\{100, 500\}$ with learning rates of $\{0.01, 0.05, 0.1\}$, except for the versions of NELL datasets, where $d = 200$ was used. This was done to show

the effectiveness of the model in different dimensions. The considered batch sizes for all datasets are $\{100, 500, 1000, 2000\}$. Regularization coefficients are tested among $\{0.01, 0.05, 0.1, 0.5\}$. For all the required values in our evaluation tables, which were not reported in the original papers, we trained the models and reported our findings. To train models on NELL-995-h25, NELL-995-h50, NELL-995-h75 and NELL-995-h100, we proceeded as follows: First, the

Dataset	#training	#validation	#test
FB15k	483,142	50,000	59,071
WN18	141,442	5,000	5,000
FB15k-237	272,115	17,535	20,466
WN18RR	86,835	3,034	3,134
NELL-995-h25	122,618	9,194	9,187
NELL-995-h50	72,767	5,440	5,393
NELL-995-h75	59,135	4,441	4,389
NELL-995-h100	50,314	3,763	3,746

Table 6: **Dataset Statistics.** Split of datasets in terms of number of triples.

NELL-995-h25 dataset was used to find the best hyperparameter setting among the aforementioned hyperparameter settings. After the best setting is found per model, the same hyperparameters for each model are applied to NELL-995-h50, NELL-995-h75 and NELL-995-h100. The same fixed hyperparameters per model are then also used when training a NELL-995-h25 model with a different embedding dimension.

Proof of Subsumption (Proposition 1)

In this part, we prove that $5^\star E$ subsumes five popular KGE models namely DistMult, ComplEx, pRotatE, RotatE and TransE. Here, we provide proofs for the following items:

(a) $5^\star E$ subsumes DistMult with its original score function $f(h, r, t) = Re(\langle \mathbf{h}_r, \bar{\mathbf{t}} \rangle)$, where

$$\mathbf{h}_r = [\mathbf{h}_{r1}, \dots, \mathbf{h}_{rd}], \mathbf{h}_{ri} = g_r(\mathbf{h}_i) \doteq \mathfrak{S}_{ri}[\mathbf{h}_i, 1]^T, \quad i = 1, \dots, d. \quad (12)$$

Note that here we use homogeneous coordinates. With the symbol \doteq , we mean that the left hand side of Equation 12 (i.e. $g_r(\mathbf{h}_i)$) equals the results of the right hand side after dehomogenization.

(b) $5^\star E$ subsumes pRotatE with its original score function $f(h, r, t) = Re(\langle \mathbf{h}_r, \bar{\mathbf{t}} \rangle)$.

(c) $5^\star E$ subsumes ComplEx with its original score function $f(h, r, t) = Re(\langle \mathbf{h}_r, \bar{\mathbf{t}} \rangle)$.

(d) $5^\star E$ subsumes RotatE with score function $f(h, r, t) = -\|\mathbf{h}_r - \mathbf{t}\|$ (changed inner product to distance).

(e) $5^\star E$ subsumes TransE with score function $f(h, r, t) = -\|\mathbf{h}_r - \mathbf{t}\|$ (changed inner product to distance).

Proof. (a) From equation 12, we have

$$\mathbf{h}_{ri} = g_r(\mathbf{h}_i) \doteq \mathfrak{S}_{ri}[\mathbf{h}_i, 1]^T, i = 1, \dots, d,$$

where $\mathfrak{S}_{ri} = \begin{bmatrix} \mathbf{r}_{ai} & \mathbf{r}_{bi} \\ \mathbf{r}_{ci} & \mathbf{r}_{di} \end{bmatrix}$. Let $Im(\mathbf{r}_{ai}) = Im(\mathbf{r}_{bi}) = Im(\mathbf{r}_{ci}) = Im(\mathbf{r}_{di}) = Im(\mathbf{h}_i) = Re(\mathbf{r}_{ci}) = Re(\mathbf{r}_{bi}) = 0$, and $Re(\mathbf{r}_{di}) = 1$. Therefore, we have

$$\begin{aligned} \mathbf{h}_{ri} &= g_r(\mathbf{h}_i) \doteq \mathfrak{S}_{ri}[\mathbf{h}_i, 1]^T = \begin{bmatrix} \mathbf{r}_{ai} & 0 \\ 0 & 1 \end{bmatrix} [\mathbf{h}_i, 1]^T \\ &= [\mathbf{r}_{ai}\mathbf{h}_i, 1]^T, i = 1, \dots, d, \end{aligned}$$

from which we conclude $\mathbf{h}_{ri} = \mathbf{r}_{ai}\mathbf{h}_i$ after dehomogenization. Therefore, the score function is defined as

$$f(h, r, t) = Re(\langle \mathbf{h}_r, \bar{\mathbf{t}} \rangle) = \sum_{i=1}^d (\mathbf{h}_i \mathbf{r}_{ai} \bar{\mathbf{t}}_i) = f^{DistMult}(h, r, t). \text{ From these equality in quotations, we conclude that DistMult is a special case of } 5^\star E \text{ and therefore, is subsumed by } 5^\star E. \quad \square$$

Proof. (b) From Equation 12, we can derive

$$\mathbf{h}_{ri} = g_r(\mathbf{h}_i) \doteq \mathfrak{S}_{ri}[\mathbf{h}_i, 1]^T, i = 1, \dots, d,$$

where $\mathfrak{S}_{ri} = \begin{bmatrix} \mathbf{r}_{ai} & \mathbf{r}_{bi} \\ \mathbf{r}_{ci} & \mathbf{r}_{di} \end{bmatrix}$. Now, if we assume $Im(\mathbf{r}_{bi}) = Im(\mathbf{r}_{ci}) = Im(\mathbf{r}_{di}) = Re(\mathbf{r}_{ci}) = Re(\mathbf{r}_{bi}) = 0$, and $Re(\mathbf{r}_{di}) = 1$, and $|\mathbf{r}_{ai}| = |\mathbf{h}_i| = |\mathbf{t}_i| = 1$. Consequently, we can conclude

$$\begin{aligned} \mathbf{h}_{ri} &= g_r(\mathbf{h}_i) \doteq \mathfrak{S}_{ri}[\mathbf{h}_i, 1]^T = \begin{bmatrix} \mathbf{r}_{ai} & 0 \\ 0 & 1 \end{bmatrix} [\mathbf{h}_i, 1]^T \\ &= [\mathbf{r}_{ai}\mathbf{h}_i, 1]^T, i = 1, \dots, d. \end{aligned}$$

Therefore, we end up with $\mathbf{h}_{ri} = \mathbf{r}_{ai}\mathbf{h}_i$ after dehomogenization. This leads us to define the score function as $f(h, r, t) = Re(\langle \mathbf{h}_r, \bar{\mathbf{t}} \rangle) = \sum_{i=1}^d Re(\langle \mathbf{h}_{ri}, \bar{\mathbf{t}}_i \rangle) = \sum_{i=1}^d Re(\mathbf{h}_{ri})Re(\bar{\mathbf{t}}_i) + Im(\mathbf{h}_{ri})Im(\bar{\mathbf{t}}_i)$ which is equivalent with the pRotatE score function (Sun et al. 2019) i.e. $f(h, r, t) = -\|\mathbf{h}_r - \mathbf{t}\|$ because $|\mathbf{r}_{ai}| = |\mathbf{h}_i| = |\mathbf{t}_i| = 1$ (the length of modulus of each elements of embedding vector for entities and relations does not participate in computation of score of triples). \square

Proof. (c) From Equation 12, we have

$$\mathbf{h}_{ri} = g_r(\mathbf{h}_i) \doteq \mathfrak{S}_{ri}[\mathbf{h}_i, 1]^T, i = 1, \dots, d,$$

where $\mathfrak{S}_{ri} = \begin{bmatrix} \mathbf{r}_{ai} & \mathbf{r}_{bi} \\ \mathbf{r}_{ci} & \mathbf{r}_{di} \end{bmatrix}$. Let $Im(\mathbf{r}_{bi}) = Im(\mathbf{r}_{ci}) = Im(\mathbf{r}_{di}) = Re(\mathbf{r}_{ci}) = Re(\mathbf{r}_{bi}) = 0$, and $Re(\mathbf{r}_{di}) = 1$.

From these assumptions, we can conclude

$$\begin{aligned} \mathbf{h}_{ri} &= g_r(\mathbf{h}_i) \doteq \mathfrak{S}_{ri}[\mathbf{h}_i, 1]^T = \begin{bmatrix} \mathbf{r}_{ai} & 0 \\ 0 & 1 \end{bmatrix} [\mathbf{h}_i, 1]^T \\ &= [\mathbf{r}_{ai}\mathbf{h}_i, 1]^T, i = 1, \dots, d, \end{aligned}$$

where after dehomogenization, we have $\mathbf{h}_{ri} = \mathbf{r}_{ai}\mathbf{h}_i$. From these and the assumption of $f(h, r, t) = Re(\langle \mathbf{h}_r, \bar{\mathbf{t}} \rangle)$ as the base score function, we then prove $f(h, r, t) = Re(\langle \mathbf{h}_r, \bar{\mathbf{t}} \rangle) = \sum_{i=1}^d Re(\langle \mathbf{h}_i, \mathbf{r}_{ai}, \bar{\mathbf{t}}_i \rangle) = f^{ComplEx}(h, r, t)$. Therefore, this shows that the ComplEx model is a special case in a variant of $5^\star E$ with score function of $f(h, r, t) = Re(\langle \mathbf{h}_r, \bar{\mathbf{t}} \rangle)$. This also means that ComplEx is subsumed by $5^\star E$. \square

Proof. (d) From Equation 12, we have

$$\mathbf{h}_{ri} = g_r(\mathbf{h}_i) \doteq \mathfrak{S}_{ri}[\mathbf{h}_i, 1]^T, i = 1, \dots, d,$$

where $\mathfrak{S}_{ri} = \begin{bmatrix} \mathbf{r}_{ai} & \mathbf{r}_{bi} \\ \mathbf{r}_{ci} & \mathbf{r}_{di} \end{bmatrix}$. Let $Im(\mathbf{r}_{bi}) = Im(\mathbf{r}_{ci}) = Im(\mathbf{r}_{di}) = Re(\mathbf{r}_{bi}) = Re(\mathbf{r}_{ci}) = 0$, and $Re(\mathbf{r}_{di}) = 1$.

1, $|\mathbf{r}_{ai}| = 1$. We then have

$$\begin{aligned}\mathbf{h}_{ri} &= g_r(\mathbf{h}_i) \doteq \mathfrak{S}_{ri}[\mathbf{h}_i, 1]^T = \begin{bmatrix} \mathbf{r}_{ai} & 0 \\ 0 & 1 \end{bmatrix} [\mathbf{h}_i, 1]^T \\ &= [\mathbf{r}_{ai}\mathbf{h}_i, 1], i = 1, \dots, d.\end{aligned}$$

With $f(h, r, t) = -\|\mathbf{h}_r - \mathbf{t}\|$ as score function, we have $f(h, r, t) = -\|\mathbf{h}_r - \mathbf{t}\| = -\|\mathbf{h} \circ \mathbf{r}_a - \mathbf{t}\| = f^{\text{RotatE}}(h, r, t)$. Therefore, RotatE is a special case of in a variant of 5★E with score function of $f(h, r, t) = -\|\mathbf{h}_r - \mathbf{t}\|$ and is subsumed by it. \square

Proof. (e) From Equation 12, we conclude

$$\mathbf{h}_{ri} = g_r(\mathbf{h}_i) \doteq \mathfrak{S}_{ri}[\mathbf{h}_i, 1]^T, i = 1, \dots, d,$$

where $\mathfrak{S}_{ri} = \begin{bmatrix} \mathbf{r}_{ai} & \mathbf{r}_{bi} \\ \mathbf{r}_{ci} & \mathbf{r}_{di} \end{bmatrix}$. Here, we assume $Im(\mathbf{r}_{ai}) = Im(\mathbf{r}_{bi}) = Im(\mathbf{r}_{ci}) = Im(\mathbf{r}_{di}) = Re(\mathbf{r}_{ci}) = 0$, and $Re(\mathbf{r}_{ai}) = Re(\mathbf{r}_{di}) = 1$. This assumption leads us to have

$$\begin{aligned}\mathbf{h}_{ri} &= g_r(\mathbf{h}_i) \doteq \mathfrak{S}_{ri}[\mathbf{h}_i, 1]^T = \begin{bmatrix} 1 & \mathbf{r}_{bi} \\ 0 & 1 \end{bmatrix} [\mathbf{h}_i, 1]^T \\ &= [\mathbf{h}_i + \mathbf{r}_{bi}, 1], i = 1, \dots, d.\end{aligned}$$

After dehomogenization, we have $\mathbf{h}_{ri} = \mathbf{h}_i + \mathbf{r}_{bi}$ which consequently gives $f(h, r, t) = -\|\mathbf{h}_r - \mathbf{t}\| = -\|\mathbf{h} + \mathbf{r}_b - \mathbf{t}\| = f^{\text{TransE}}(h, r, t)$. Therefore, it is proven that the TransE model is a special case in a variant of 5★E with score function of $f(h, r, t) = -\|\mathbf{h}_r - \mathbf{t}\|$. This means that 5★E subsumes by TransE. \square

Proof of Full Expressiveness (Corollary 1)

Here we prove that the 5★E model is fully expressive.

Proof. We divide the proof into two argumentation steps:

First, we show that 5★E can express any ranking tensor $\mathcal{A} \in \mathbb{R}^{n_e \times n_e \times n_r}$, where n_e, n_r are the number of entities and relations in a KG respectively. α_{ikj} is the ikj th element of the tensor \mathcal{A} that corresponds to the triple (h_i, r_k, t_j) . For a triple (h_i, r_k, t_j) which is scored higher than a triple (h'_i, r'_k, t'_j) by the model, the ranking tensor gives a lower rank to (h_i, r_k, t_j) than to (h'_i, r'_k, t'_j) . More details can be found in (Wang, Gemulla, and Li 2018).

Second, for any boolean tensor $\mathcal{B} \in \{0, 1\}^{n_e \times n_e \times n_r}$, there is a ranking matrix obtained by the 5★E model which is consistent with the boolean tensor. More precisely, if we assume $\beta_{ikj} = 1$ where (h_i, r_k, t_j) is a positive triple, and $\beta_{i'k'j'} = 0$ where (h'_i, r'_k, t'_j) is a negative triple, then we have $\alpha_{i'k'j'} < \alpha_{ikj}$.

The first two argumentation steps allow to conclude that 5★E is fully expressive, i.e. capable of representing any ground truth over triples of a KG.

Here, we provide the proofs for expressiveness by explaining the steps in detail.

For the proof of the first argumentation, let $\mathcal{M}_m \in \mathbb{R}^{n_e \times n_r \times n_e}$ be the tensor corresponding to the score function of the model m obtained by an assignment to embeddings

of entities and relations in a \mathcal{KG} . The ikj -th element of \mathcal{M}_m is denoted by μ_{ikj} that equals to the score of a model m for a triple (h_i, r_k, t_j) i.e. $\mu_{ikj} = f^m(h_i, r_k, t_j)$. Given a score tensor \mathcal{M}_m , the corresponding ranking tensor \mathcal{A}_m is obtained by applying a mapping $\phi : \mathbb{R}^{n_e \times n_r \times n_e} \rightarrow \mathbb{N}^{n_e \times n_r \times n_e}$ in that $\mu_{i'k'j'} \leq \mu_{ikj} \leftrightarrow \alpha_{i'k'j'} = \phi(\mu_{i'k'j'}) \geq \alpha_{ikj} = \phi(\mu_{ikj})$. The authors of (Wang, Gemulla, and Li 2018) prove that the ComplEx model is universal i.e. given any ranking matrix \mathcal{A} , there are assignments to embedding vectors such that the obtained score tensor fulfills $\mathcal{A} = \phi(\mathcal{M}_{\text{ComplEx}})$.

In the subsumption proof case (c), we proved that 5★E subsumes ComplEx, therefore, for any given ranking matrix \mathcal{A} there is a vector assignment to embeddings of entities and relations such that the score of triples create a tensor that satisfies

$$\mathcal{A} = \phi(\mathcal{M}_{5\star E}).$$

The authors of (Wang, Gemulla, and Li 2018) show that for a given boolean matrix \mathcal{B} , there is a ranking matrix which is consistent with the boolean matrix. Therefore, for any given boolean matrix \mathcal{B} , there exists a ranking $\mathcal{A} = \phi(\mathcal{M}_{5\star E})$ which is consistent with it.

From the first and second argument, we conclude that for any given ground truth over a \mathcal{KG} , there is an assignment to embeddings of entities and relations in the \mathcal{KG} such that 5★E separates the correct triples from incorrect ones. This means that 5★E is fully expressive. \square

Proof of Pattern Inference (Propositions 2, 3, 4, 5)

Here we prove that our model is able to infer symmetric, inverse, composition and reflexive patterns.

(f) Let $r_1, r_2, r_3 \in \mathcal{R}$ be relations such that r_3 is a composition (e.g. *UncleOf*) of r_1 (e.g. *BrotherOf*) and r_2 (e.g. *FatherOf*). 5★E infers composition with $\mathfrak{S}_{r_1} \mathfrak{S}_{r_2} = \mathfrak{S}_{r_3}$.

(g) Let $r_1 \in \mathcal{R}$ be the inverse of $r_2 \in \mathcal{R}$. 5★E infers this pattern with $\mathfrak{S}_{r_1} = \mathfrak{S}_{r_2}^{-1}$.

(h) Let $r \in \mathcal{R}$ be symmetric. 5★E infers the symmetric pattern if $\mathfrak{S}_r = \mathfrak{S}_r^{-1}$.

(i) Let $r \in \mathcal{R}$ be a reflexive relation. In dimension d , 5★E infers reflexive patterns with $O(2^d)$ distinct representations of entities if the fixed points of the involved transformations are non-identical.

Here we provide the proofs of the aforementioned propositions for pattern inference. We use the following proposition from (Kisil 2012) in our proof:

Proposition 6. (Kisil 2012) *Let $\mathfrak{S}_{r_1}, \mathfrak{S}_{r_2}$ be matrices of two projective transformations τ_{r_1}, τ_{r_2} , which are respectively associated to two Möbius transformations $\vartheta_{r_1}, \vartheta_{r_2}$. The product of the two matrices results in a matrix $\mathfrak{S}_{r_3} = \mathfrak{S}_{r_1} \mathfrak{S}_{r_2}$, which is associated to a projective transformation τ_3 corresponding to the composition of the two Möbius transformations $\vartheta_{r_3} = \vartheta_{r_1} \circ \vartheta_{r_2}$.*

Given this proposition, we can then continue:

Proof. (f). A relation r_3 is composed from two relations

r_1, r_2 if

$$\forall e_1, e_2, e_3 \in \mathcal{E}, (e_1, r_1, e_2) \wedge (e_2, r_2, e_3) \rightarrow (e_1, r_3, e_3). \quad (13)$$

A model infers a composition pattern when for given entities e_1, e_2, e_3 , if the score of the model represents triples (e_1, r_1, e_2) and (e_2, r_2, e_3) as positive, it also represents (e_1, r_3, e_3) as positive, that is

$$\begin{aligned} g_{r1}(\mathbf{e}_{1i}) &= \mathbf{e}_{2i}, \\ g_{r2}(\mathbf{e}_{2i}) &= \mathbf{e}_{3i}, \end{aligned} \quad (14)$$

then $g_{r3}(\mathbf{e}_{1i}) = \mathbf{e}_{3i}, i = 1, \dots, d$, where

$$g_{ri}(\mathbf{h}_i) = \vartheta(\mathbf{h}_i, \mathbf{r}_i) = \frac{\mathbf{r}_{ai}\mathbf{h}_i + \mathbf{r}_{bi}}{\mathbf{r}_{ci}\mathbf{h}_i + \mathbf{r}_{di}}, \mathbf{r}_{ai}\mathbf{r}_{di} - \mathbf{r}_{bi}\mathbf{r}_{ci} \neq 0, \quad (15)$$

$$i = 1, \dots, d.$$

From Equations 14, we insert $\mathbf{e}_{2i} = g_{r1}(\mathbf{e}_{1i})$ into $g_{r2}(\mathbf{e}_{2i}) = \mathbf{e}_{3i}$, which gives $g_{r2}(g_{r1}(\mathbf{e}_{1i})) = \mathbf{e}_{3i}$. Therefore, we have

$$g_{r2} \circ g_{r1}(\mathbf{e}_{1i}) = \mathbf{e}_{3i}.$$

This means two Möbius transformations g_{r2}, g_{r1} are composed. Considering the Proposition 6, and assuming $\mathfrak{S}_{r3} = \mathfrak{S}_{r1}\mathfrak{S}_{r2}$, we have $g_{r2} \circ g_{r1}(\mathbf{e}_{1i}) = g_{r3}(\mathbf{e}_{1i}) = \mathbf{e}_{3i}$. This means that the triple (e_1, r_3, e_3) must be positive (= inferred to be positive).

Note that the above mentioned proof holds for the case where $g_r(\mathbf{h}_{ri}) = \mathbf{t}_i, i = 1, \dots, d$ which concludes that a triple (h, r, t) is positive. It also holds for the case that imaginary parts of embeddings become zero.

With assumption $g_r(\mathbf{h}_{ri}) = \bar{\mathbf{t}}_i, i = 1, \dots, d$, the imaginary part of \mathbf{e}_{2i} must be zero. \square

Proof. (g). A relation r_2 is inverse of relation r_1 if

$$\forall e_1, e_2 \in \mathcal{E}, (e_1, r_1, e_2) \rightarrow (e_2, r_2, e_1). \quad (16)$$

A model infers the inverse pattern for given entities e_1, e_2 , if the following holds: If (e_1, r_1, e_2) are represented as positive, then (e_2, r_2, e_1) as positive are also represented as positive. This can be formulated as

$$g_{r1}(\mathbf{e}_{1i}) = \mathbf{e}_{2i}, \quad (17)$$

then $g_{r2}(\mathbf{e}_{2i}) = \mathbf{e}_{1i}$.

From Equation 17, we have $\mathbf{e}_{2i} = g_{r1}(\mathbf{e}_{1i})$. Since g_{r1} is Möbius and is invertible, and $\mathfrak{S}_{r1} = \mathfrak{S}_{r2}^{-1}$ (from the assumption), we have

$$\mathbf{e}_{2i} = g_{r2}^{-1}(\mathbf{e}_{1i}).$$

Therefore, we have

$$\mathbf{e}_{1i} = g_{r2}(\mathbf{e}_{2i}).$$

This means that the triple (e_2, r_2, e_1) must be positive (inferred as positive).

When $g_r(\mathbf{h}_{ri}) = \mathbf{t}_i, i = 1, \dots, d$ (denoting triple (h, r, t) is positive), the above-mentioned proof holds. The proof also

holds for the case that the imaginary part of embeddings become zero.

In the case that the equality $g_r(\mathbf{h}_{ri}) = \bar{\mathbf{t}}_i, i = 1, \dots, d$, the previous assumption is changed to $\mathfrak{S}_2 = \mathfrak{S}_1^{-1}$. \square

Proof. (h). A relation r is symmetric if

$$\forall e_1, e_2 \in \mathcal{E}, (e_1, r, e_2) \rightarrow (e_2, r, e_1). \quad (18)$$

A model infers a symmetric pattern when for given entities e_1, e_2 , the following holds: If the model represents triples (e_1, r, e_2) as positive, then it also represents (e_2, r, e_1) as positive. This can be formulated as

$$g_r(\mathbf{e}_{1i}) = \mathbf{e}_{2i}. \quad (19)$$

From this and taking Equation 18 into account, we have $g_r(\mathbf{e}_{2i}) = \mathbf{e}_{1i}$.

From Equation 19, we have

$\mathbf{e}_{2i} = g_r(\mathbf{e}_{1i})$. Since g_r is Möbius, and $\mathfrak{S}_r = \mathfrak{S}_r^{-1}$ (from the assumption), we have

$$\mathbf{e}_{2i} = g_r^{-1}(\mathbf{e}_{1i}).$$

Therefore, we have

$$\mathbf{e}_{1i} = g_r(\mathbf{e}_{2i}).$$

This means that the triple (e_2, r, e_1) must be positive (= inferred as positive).

Note that the above mentioned proof is held when $g_r(\mathbf{h}_{ri}) = \mathbf{t}_i, i = 1, \dots, d$. From this, we conclude that a triple (h, r, t) is positive. It also holds for the case that the imaginary part of embeddings become zero.

When $g_r(\mathbf{h}_{ri}) = \bar{\mathbf{t}}_i, i = 1, \dots, d$ holds, the assumption is changed to $\mathfrak{S} = \bar{\mathfrak{S}}^{-1}$. \square

Proof. (i). Let r be reflexive. We have $\mathbf{e}_{ri} = \mathbf{e}_i, i = 1, \dots, d$. Because \mathbf{e}_{ri} is a Möbius transformation of the head, the formula $\mathbf{e}_{ri} - \mathbf{e}_i = 0$ gives its fixed points. As each Möbius transformation has at most two fixed points, we can therefore conclude that there are $O(2^d)$ distinct representations for entities in a KG that allow to infer a reflexive pattern. When the imaginary part of the embeddings is zero, the above mentioned proof holds for $\mathbf{e}_{ri} = \bar{\mathbf{e}}_i$. \square

Learned Transformation Functions. Figure 15 illustrates the results of learned transformation functions for various relations in WordNet. Sub-figure (a) and (b) refer to the *hyponym* relation. However, the depicted shape of transformation function differs for hyperbolic and elliptic transformations. This confirms the flexibility of the model in embedding various graph structures as well as diversity in density/sparsity of flow (e.g., *hyponym* relation). We also observed that when two pairs of relations form inverse patterns (in the same dimension), the model mainly learns the same transformation functions but with different directions.